

Overview of accelerated aging and polymer degradation kinetics for combined radiation-thermal environments

Mathew Celina*, Erik Linde, Douglas Brunson, Adam Quintana, Nicholas Giron

Sandia National Laboratories, Organic Materials Science Dept.1853, Albuquerque, NM, 87185-1411, USA



ARTICLE INFO

Article history:

Received 1 March 2019

Received in revised form

12 June 2019

Accepted 12 June 2019

Available online 15 June 2019

Keywords:

Accelerated polymer aging
Radiation-thermal oxidative degradation
Predictive kinetic models
Aging model evaluation
Cable insulation performance under combined environments

ABSTRACT

Polymer aging under combined radiation-thermal oxidative conditions is intrinsically more convoluted than traditional thermal degradation. Accelerated aging methods for predictive purposes have to include thermal as well as radiative degradation pathways that initially may be regarded as independent parallel processes without additional synergism. Material aging is therefore represented as the sum of a thermal and radiative contribution. Data from accelerated aging may be available as dose to equivalent damage (DED) or degradation rates, yet they require different analytical approaches to yield the underlying temperature dependence and its activation energy. Further, kinetic models that embrace combined pathways can offer guidance for extrapolation of accelerated to ambient conditions, enabling the prediction of material aging behavior or remaining performance margins for requalification purposes. The existing theoretical approaches, their implications and an alternative option for globally fitting experimental data sets to kinetic aging models for combined environments are reviewed. This overview offers a pragmatic approach towards an expanded interpretation of oxidation rate and aging data properties for combined environments, all the way to time-dependence for rates and synergistic contributions. Further evidence is provided that for some material behaviors an additional E_a for the radiative term under high dose rate conditions could be beneficial, as similarly expressed by increases in a synergistic interaction parameter. Improved kinetic aging models are derived and applied to a comprehensive set of experimental oxidation rates for a chlorosulfonated polyethylene material. Emphasized is also the issue that initial oxidation rates versus superposition of oxidation levels (integrated rates) may result in slightly different thermal E_a values through added time dependency. Constant oxidation rates relate to an exponential decay in elongation at break data. Aging predictions can be improved through measured oxidation rates, a systematic understanding of material behavior over a large dose rate - temperature regime, and application of an appropriate aging model. The most general aging model will contain a radiative E_a , time-dependence of rate, and added synergism that may grow with temperature.

© 2019 Elsevier Ltd. All rights reserved.

Contents

1. Introduction	354
2. Experimental approach for degradation rates under radiation -thermal conditions	355
3. Combined radiation-thermal degradation models	356
3.1. General definitions	356
3.2. DED - degradation rate model with single thermal E_a	356
3.3. Empirical degradation rate - DED model with additional temperature dependence for radiative term	358
3.4. Superposition of DED or degradation rates to yield E_a	360
3.5. Enhanced degradation rate – DED model with independent E_a 's for thermal and radiative components	362
4. Oxidation rates analyses with four different models	363
5. Interpretation of thermal E_a for specific cable insulation material	365

* Corresponding author. Sandia National Laboratories , PO Box 5800, MS 1411, Organic Materials Science Dept. 1853, Albuquerque, NM, 87185, USA.

E-mail address: mccelin@sandia.gov (M. Celina).

5.1. Time dependence for oxidation/degradation rate	367
5.2. Constant versus declining thermal oxidation/degradation rate	367
5.3. Relationship between activation energies for thermal degradation	367
5.4. General radiation-thermal model with a declining rate (example: power law)	369
6. Performance predictions for combined radiation-thermal conditions based on oxidation rates	369
7. Approaches towards synergism between radiative and thermal pathways	373
8. Conclusions	376
8.1. Avenues for expanded combined environment aging models	376
8.2. Determination of activation energies and validation of aging model	376
8.3. Determination of E_a at fixed dose rate has no predictive value	376
8.4. Complications when oxidation rates show subtle time behavior	376
8.5. Better performance predictions based on oxidation behavior	376
8.6. Synergism between radiation and thermal pathways	377
8.7. Current status and forward looking directions	377
Acknowledgements	377
References	377

1. Introduction

The prediction and a rigorous understanding of materials performance under combined radiation-thermal environments is of ongoing interest to the polymer aging community. It is widely accepted that the degradation processes are convoluted when aging occurs under simultaneous radiation and thermal exposure conditions, as for example encountered during long-term use conditions in nuclear power plants or related applications [1–12]. Polymer aging in such situations is not simply an issue of thermal exposure alone, but will proceed within the boundaries of purely thermally driven or radiation dominated degradation pathways at high dose rate conditions. This also implies that accelerated aging for predictive purposes cannot be conducted by simply raising the temperature as is usually done for thermal aging studies [13–15], but must accommodate radiation exposure in parallel [14,16]. For accelerated aging studies to be truly predictive they must relate to the underlying polymer science, and we also have to recognize some common limitations. Most importantly, when aging is conducted under oxidative conditions, diffusion limited oxidation (DLO) effects may need to be eliminated or carefully interpreted, as these effects complicate if not prevent the extrapolation of material property changes from highly accelerated to ambient use conditions [13,14,17]. Further, it is not easy to measure degradation rates directly and therefore rather the effects of aging are often monitored under accelerated aging conditions, for example as changes in mechanical properties such as tensile elongation [5,14,16].

Several methods have been proposed to enable lifetime predictions and offer perspectives on material degradation behavior based on accelerated polymer aging studies [13,14,16]. A class of materials of sustained interest to the polymer aging community are cable insulation materials for nuclear power plant applications, with the focus ranging from a mechanistic understanding of degradation processes and their chemical signatures to antioxidant interaction and accelerated aging techniques for predictive purposes [5,11,12,18–24]. Accurately estimating the lifetimes or remaining performance of these materials for requalification purposes [6] is challenging because they are subjected to both thermally and radiation driven degradation while in use under combined environmental conditions, meaning conditions that are usually not covered by ‘short term’ accelerated aging studies. The general approach is to gather cumulative aging data in air which characterizes the extent of degradation of the material under elevated temperatures and dose rates, then analyze or fit the data to an aging model, and use the model to accurately extrapolate the

time required for the material to reach a critical level of degradation under use conditions. An aging state of concern is defined by a particular characteristic of the material indicating failure and should represent a relevant performance expectation agreed upon through consultations between polymer scientists and design/facility engineers. This criterion may be a 50% reduction of relative elongation at break [25], meaning it reaches its lifetime when it breaks at 50% of maximum elongation in its unaged state. Similarly, minimum performance criteria have been defined as 50 or 100% residual absolute elongation at break, the latter being a more conservative approach for lifetime prediction purposes [5].

Methods proposed in the literature dealing with accelerated aging and lifetime prediction for polymers usually focus on the use of data superposition approaches in order to determine the thermal activation energy, commonly denoted E_a . Since temperature is the main driver of degradation under low to moderate dose rate conditions (<100 Gy/h) and is also the easiest way to accelerate the degradation rate, it is clear that knowing the underlying thermal E_a will help us predict degradation rates at ambient conditions. Additional complexity arises with radiation driven pathways and whether those occur as a simple addition to thermal reactions or whether they may have their own temperature dependence. Further, additional synergism may occur for simultaneous thermal and radiative degradation including more complex temperature dependence.

It has often been suggested that radiation chemistry is driven primarily by dose rate through free radical initiation reactions, subsequent hydrogen abstraction and primary chain scission or crosslinking, and that such reactions have low activation energy [26–30]. However, oxidation of a material also involves secondary chemistry with follow-up hydroperoxide decomposition, free radical transfer reactions, volatile evolution (short chain fragments), and more complex polymer scission/crosslinking chemistry which drives material property changes commonly encountered as loss of elongation. This means that oxidative degradation involves successive reaction steps, beyond simple radiation initiation and hydroperoxide formation. Crosslinking and scission will often occur in parallel and its ratio is material and temperature specific. For crosslinked polyolefin materials oxidative chain scission is the dominant degradation pathway which results in reduced elasticity [5,31], with some crosslinking occurring in parallel and usually becoming more important with temperature or under non-oxidative (inert) conditions [32,33]. In comparison, most elastomeric materials containing unsaturation tend to crosslink under oxidative conditions, leading to increased modulus and hardening

with embrittlement [17,34–41]. We also recognize that inert radiative processes, usually inducing additional crosslinking, may become more important as the dose rate increases, due to potential DLO but also more competitive rapid alkyl radical recombination. The latter process would be consistent with an exponent for the dose rate of less than one (as will be discussed further below), which means a growing fraction of the irradiation no longer contributes to oxidatively driven degradation when inert processes may become competitive with increasing dose rate.

There is significant evidence that radiation dominated degradation has near zero or low thermal activation energies [1,3,16], yet there is a priori no justification that radiation dominated oxidative degradation should not have limited temperature dependence. Zero activation energy for all radiatively initiated oxidation processes may not necessarily be consistent with other experimental evidence, considering the low thermal activation energies encountered for accelerated UV exposure (scission dominated photo-oxidation chemistry) [42–44], and also associated with diffusion of small molecules (free radical transfer reactions) and related mobility aspects as part of degradation reactions [45,46]. In fact, in some earlier studies on PVC or PE [8,47,48], it was concluded that temperature contributed at high dose rates as it affected post-initiation hydroperoxide driven follow-up chemistry. For the definition of appropriate aging models it should be considered whether for some materials combined degradation pathways could be better described by a combination of two activation energies. This was suggested by Burnay as a coupled secondary radiative E_a and exponent for dose rate of 0.95 for a high temperature elastomer (see Eq. (3) in section 3.3 for exponent on dose rate) [49]. An exponent of less than one for the dose rate means that the 'oxidative effectiveness' of the irradiation decreases with increasing dose rates and results in lower oxidation rates or higher dose to equivalent damage (**DED**). Similarly, Ito on a number of occasions emphasized a separate E_a and dose rate exponent for the radiative term as a contribution of additional 'synergism' (first mentioned with E_a 's on the order of 9–12 kJ/mol and exponent of 0.9 for PTFE-PP [50], and an E_a of 8 kJ/mol for EPR [51,52]). A more recent publication discussed thermal-radiative synergism with E_a 's on the order of 8–52 kJ/mol and dose rate exponents in the range of 0.85–0.97 [53]. However, no further evidence was offered how these numbers had been obtained. Most importantly, neither the work by Gillen [1,3,16], Burnay [49] nor Ito [51–54] defined the nature of synergism in a functional form, with the key difference in their opinions being the need or absence for a secondary radiative E_a in combined environment aging behavior.

Other important tasks, particularly for the practitioner dealing with accelerated aging and lifetime prediction or ongoing performance qualification for materials aging under combined radiation-thermal conditions [5–7], are to clarify differences in activation energies and to develop appropriate strategies for accelerated aging studies and best data analysis for predictive purposes. Improved methods have recently been offered from an experimental point of view, but not with a clearly defined aging model that covers time-dependence in degradation rates and synergism [14,16]. Previous work has mostly focused on empirical superposition analyses of **DED** data [1,3,49] and recommendations for more meaningful exposure conditions (matched accelerated conditions) [14,16], yet the current mathematical framework is limited, particularly for time dependent degradation rates and potential synergistic effects. A comprehensive theoretical framework would enable us to better compare data analyses and emphasize some of the shortcomings and challenges for more meaningful accelerated aging under combined conditions.

For practical purposes, accelerated aging may be conducted at a given dose rate for various temperatures, or for a given temperature

at different dose rates. Could either one of these approaches provide simple shift factors representing aging times (i.e. degradation rate data) that will then offer predictive value? How would we transition from basic accelerated aging approaches towards predictions for ambient conditions? Which combined aging conditions provide best predictive value or what is the feedback from aging under boundary conditions (i.e. dominant thermal or radiative conditions)? These are challenges where comprehensive aging models with a rigorous description of the degradation rates and damage parameters under varying conditions will provide suitable guidance.

The aim of this study is not to focus on kinetic models with individual rate constants and detailed mechanistic aspects attempting to define the chemistry for crosslinking, scission or oxidation reactions [55–57]. We rather wish to offer a pragmatic review and additional approaches for the interpretation of overall degradation rates and aging state evolution as a function of temperature and dose rate [1,3,16,58]. We also examine degradation models that accommodate additional complexity and degrees of freedom, show an example for time-dependence in degradation rates, and define a basic concept for contributions of synergism, since it is likely that additional synergism exists for some dose rate - temperature combinations. Further, the variability in activation energies, their determination and interpretation is emphasized.

2. Experimental approach for degradation rates under radiation -thermal conditions

Oxidation rate measurements were conducted with our routine method described previously for other materials [59,60]. Cut samples of Eaton Dekoron Hypalon (chlorosulfonated polyethylene (CSPE)) jacket material were placed into ampoules of ~20 cc volume, which were then leak tested, evacuated, and filled with reference air. Sample weights were chosen dependent on the expected oxidation rate to enable sufficient sensitivity at the lower aging conditions while also preventing rapid complete oxygen consumption under the most severe aging conditions; samples ranged from 0.5 g to 4 g—the lighter the sample, the greater the dose rate or temperature to which it was exposed.

All Eaton Dekoron Hypalon jacket material samples were aged in individual ampoules under combined thermal and radiative conditions at the Sandia National Laboratories Low Intensity Cobalt Array (LICA) facility beginning on August 25, 2014 and ending on January 29, 2015. The ampoules were aged with dose rates ranging from approximately 0.5 Gy/h to 380 Gy/h at temperatures ranging from 28 to 120 °C. Dose rates were determined multiple times by CaF₂ dosimetry using specimens located directly on the surface of the small ox-uptake ampoules at the height position of the interior polymer sample. The additional absorption by the thin ampoule wall was neglected. The immersed large aging cans have a heated internal compartment which allows the ampoules to be heated in exactly the same LICA location under identical dose rate conditions. Eight parallel samples were first aged over the dose rate range at 28 °C. The same samples were then aged at 60 °C, 80 °C, 100 °C, and lastly at 120 °C. Stable temperature conditions were provided by remote temperature controllers using a thermocouple positioned in mid-height between the ampoules in the aging can. After each experiment, the changes in oxygen concentration in the ampoule (i.e. oxygen consumption) were determined using a Differential Oxygen Analyzer acquired from Sable Systems [59]. The oxygen consumption measurements were converted to rates in mol/g-s. For each temperature and dose rate condition, only two short experiments were conducted, which provided an overview for initial oxidation rates at each condition. This means that the initial oxidation rates for the Eaton Dekoron Hypalon jacket material were

measured with the intent of these screening experiments not to drift towards significant oxidation levels. Final oxidation levels were 0.1% at the lowest dose rate, 0.36% at ~50 Gy/h, and 1.7% at ~350 Gy/h, with most of the oxidation occurring for the latter dose rate at the two highest temperatures. We recognize that this approach was not ideal, since the higher temperature exposure involved samples with some amount of pre-oxidation, but was the most effective way to acquire these guiding data subject to limits in experimental scope and efforts at the time.

For each thermal data set, the samples aged at the highest dose rates (~200 Gy/h and ~380 Gy/h) were finely sectioned to avoid potential DLO effects, which might occur for samples aged at these dose rates. We believe that the additional surface area from carefully cutting the samples did not introduce complications for the material oxidation rates. In some thermal oxidation studies in the past we had noticed enhanced oxidation rates for very finely cut material, likely due to local stabilizer loss and heterogeneous degradation phenomena for very thin pointy sample fragments (this was avoided here). Please note that we used Eaton Dekoron Hypalon CSPE for the LICA experiments in the current study (designated Hyp-06 in [5,61]) and compared it with previously reported oxidation rate behavior for a Samuel Moore Dekoron Hypalon CSPE (designated Hyp-03 in [5,61]) due to unavailability of comprehensive data for both materials. However, these two materials are near identical in terms of their modulus, initial elongation and aging behavior.

3. Combined radiation-thermal degradation models

3.1. General definitions

Before interpreting existing aging model approaches in detail, we begin by emphasizing overall concepts that apply to each method in order to predict material lifetimes and behavior. In general terms and as accepted in the literature, all polymer aging under combined thermal-radiative conditions is subject to two degradation pathways and is therefore the combination of a thermal and radiative material response [1,3,16]. The following definitions are relevant to any accelerated aging study, associated data interpretation, and specific aging model. Under aging conditions in air, polymer materials will oxidize, resulting in changes to material properties, e.g. a reduction in tensile elongation. This loss of material performance over time is referred to as degradation. The rate of degradation will depend on the particular aging conditions which may range between ambient and highly accelerated conditions (i.e. high temperature and dose rate). The aging conditions are characterized by a particular aging temperature and radiation dose rate. We denote the chosen critical level of degradation, or a single failure criterion by C_f . Here we consider an oxidation level for failure; hence C_f is given in mol/g, but could also be expressed in % elongation. The overall degradation state (for polymers most often their oxidation level which also determines tensile elongation) is given by $C = t^*r$, where C is the level of degradation at aging time t , and r is the rate of degradation. For the purpose of all aging models and discussions in sections 3–4 r is regarded to be constant with time. The time required for the material to reach the amount of oxidation equivalent to damage level C under arbitrary aging conditions is called the time to equivalent damage (**TED**) and is given by $t = C/r$ [1,3]. It is possible to also define a dose to equivalent damage (**DED** [Gy]) for any damage level which is commonly given by $DED = TED^*\gamma$ where γ is the radiation dose rate (usually in Gy/h). The dose rate is usually also assumed constant during the aging period.

The change in degradation rate subject to aging at elevated temperature is described by a shift factor. The shift factor is a function of temperature which indicates how the degradation rate

of a material is accelerated/decelerated by a change in temperature above/below some reference temperature. The definition and use of this shift factor is common throughout the literature on materials aging and degradation processes [1,3,14,60,62] and varies exponentially with temperature. If the degradation rate is a function only of temperature, as is a reasonable assumption for thermal-only aging, then the degradation rate $r(T)$ can be expressed as being directly proportional to the shift factor a_T , with the proportionality constant being the degradation rate at the reference temperature $r(T_{ref})$, as shown below. The shift factor describes how the thermal degradation rate depends on temperature, and can be used in aging models, which we describe later, to extract the thermal activation energy by time-temperature shifting experimental data (hence the name ‘shift factor’).

$$r(T) = r(T_{ref}) * a_T$$

As we will explain in the remainder of this paper, models for oxidation rate as functions of both temperature and dose rate can be more complicated and it is then no longer possible to obtain a reasonable estimate of the thermal activation energy by a simple data shifting procedure. For example, such situations are encountered when inverse temperature phenomena affect the material degradation behavior [16,32,33,63]. We will therefore consider here only material oxidation in the context of degradation without any other temperature anomaly. In multiple modeling efforts that we describe below, for the sake of simplicity and our intent of offering an overview perspective, the material degradation state corresponding to failure is defined as $C_f = 6.25 \times 10^{-4} \text{ mol O}_2/(\text{g material})$, which is equivalent to 2% oxidation (2% oxygen by mass consumed by the total material [60]). While the oxidation level for failure is arbitrarily defined in this way, it is consistent with many experimental observations for elastomeric materials and allows us to consider degradation models under realistic circumstances, but mostly from a theoretical point of view as an overview focusing on modeling differences rather than a specific failure criterion. Of course, this parameter can be defined as needed for any property serving as a suitable aging state indicator.

As the goals of this study, we wish to review existing aging models, discuss their foundation, benefits and shortcomings, and the methods of data analysis currently used to determine the underlying model parameters. We wish to propose alternative models for material aging and explain their advantages in the context of oxidation rate data that we recently obtained for an Eaton Dekoron Hypalon jacketing material. The intent is to also offer a perspective on the relationship between a theoretical framework for combined environment aging versus practical needs for accelerated aging experiments and lifetime prediction. For the following discussions, all accelerated aging is deemed to occur under non-diffusion limited oxidation conditions, and absence of any inverse temperature phenomena [16,32,33,63] for the purpose of data interpretation and predictive modeling. The overall degradation rate (material oxidation) as a combination of thermal and radiative processes is transforming the material into an oxidized degraded state with a corresponding reduction in mechanical properties, for which a specific oxidation state can be correlated with material failure criterion (i.e. 2% oxidation may imply 100% residual elongation or other experimentally confirmed correlations shown later). However, specific correlations between oxidation level and mechanical properties are not required for a generalized discussion of such aging models.

3.2. DED - degradation rate model with single thermal E_a

The time-temperature-dose rate (t-T-r) superposition approach,

originally introduced by Gillen and Clough in 1989 [1] was one of the earliest comprehensive approaches dealing with radiation-thermal aging conditions and interpretation of experimental data to derive predictions for low dose rate conditions. The dose to equivalent damage (**DED**) at different temperatures is plotted against dose rate on a common log-log scale. Fig. 1 shows this basic concept for model curves of **DED** (Gy) versus dose rate (Gy/h) at four different temperatures labeled T_1 , T_2 , T_3 , and T_4 , similar to this early work [1]. We select a specific **DED** value (**DED1**) which is shown as a horizontal line. The intersections of this horizontal line with each curve are referred to as ‘isodose conditions’ because the aged material represents the same level of degradation at the elevated temperature and dose rate conditions intersecting with this line [1]. The isodose points are marked with ‘x’. At the chosen **DED1** (here 60 kGy) in Fig. 1, the points 2, 3 and 4 may each be shifted to coincide with point 1. This same shifting may be done along the horizontal line labeled **DED2** with the points 2', 3', and 4' shifted left to coincide with point 1'. In this way, shifting the **DED** curves establishes the shift factors for each **DED** value. The intent is to superpose each **DED** curve obtained at a range of temperature and dose rate conditions to the reference curve (defined by the reference temperature) by using ideally only one shift factor per temperature. The shift factor at the reference temperature T_1 is 1. If the data set over the dose rate – **DED** regime allows for superposition then the shift factors will allow for the determination of the underlying thermal E_a . For some experimental data sets, a shift along a single **DED** may not result in a single E_a but rather more complex temperature dependence.

This original approach implies that the combined radiation and thermal degradation processes will yield the shift factors independent of the particular isodose value [1]. According to Gillen and Clough, one possible functional form of the temperature and dose rate-dependent degradation rate that will allow for the dose rate superposition method described above, is when the thermal and radiative contributions to the degradation rate occur in ‘parallel non-interacting pathways’ [1]. That is, the overall degradation rate is the sum of two independent processes, one thermal and one radiative. This description was also deemed valid if a thermal-radiative rate ‘interactive’ term is uniquely defined as increasing by the same amount as when identical rate multipliers apply for temperature and dose rate conditions [1]. While this is an early reference to additional synergism, it is important to distinguish between a synergistic rate that simply increases with temperature and an independent synergistic interaction multiplier (see section 7). The functional form of such an additional ‘interactive term’ or

other rate influencing behavior in the dose-rate temperature space was not defined, but has now been described (see later sections). Earlier publications also likely implied that dose rate ($t-T-r$) superposition for **DED** data given by elongation at break is maintained, if any degradation rate changing behavior for combined environments is given by simple synergism or consistent time-dependence [1,3]. Further, for $t-T-r$ superposition to be applicable an underlying correlation must exist between oxidation level given by oxidation rate and the elongation at break condition. Hence it is important to distinguish between oxidation and its consequence, e.g. mechanical property changes.

We first consider kinetic models by excluding more complex interactive degradation pathways or time-dependent behavior, which while not published as such was the underlying requirement for idealized combined environment aging [1,3]. Although this assumes constant oxidation rates, it does not exclude systematic time dependence in the effective rate for changes in elongation, which for example may display exponential behavior (see section 6). Such models also do not accommodate variations in the oxidation level to elongation correlation, i.e. any differences in the efficiency of degradation chemistry subject to thermal or radiative boundaries. While changes in elongation can be more complicated and additional dose rate or temperature dependence can certainly be convoluting (mechanistic changes, see recent overview [16]), we believe it is also important to reflect on the underlying material oxidation behavior and its description by global kinetic models.

Kinetic models are given by the general form Eq. (1), where the first term on the right hand side represents the thermal contribution, and the second term represents the radiative contribution to the degradation rate.

$$r(T, \gamma) = r(T_{ref}, 0) * \exp\left(\frac{E_a}{R} \left(\frac{1}{T_{ref}} - \frac{1}{T}\right)\right) + f(\gamma) \quad (1)$$

For this definition, E_a is the thermal rate activation energy, R is the universal gas constant, and $f(\gamma)$ is an increasing function only of dose rate which is equal to zero when $\gamma = 0$. Substituting this expression into the definition of **DED** given in section 3.1, it follows that

$$DED(T, \gamma) = \frac{C\gamma}{r(T_{ref}, 0) * \exp\left(\frac{E_a}{R} \left(\frac{1}{T_{ref}} - \frac{1}{T}\right)\right) + f(\gamma)} \quad (2)$$

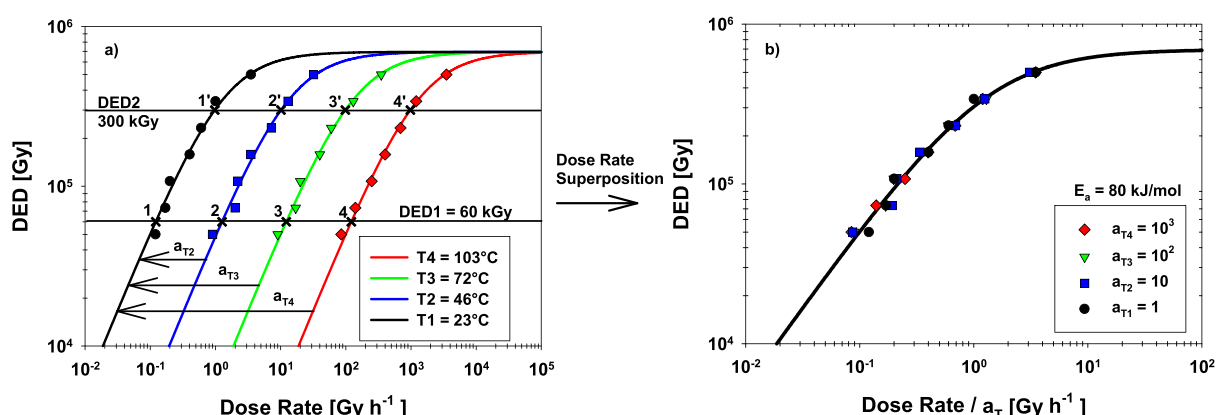


Fig. 1. a) Illustrative **DED** plots demonstrating the concept of horizontal dose rate superposition. The shift factor (a_T) for the reference temperature (T_1) is always 1 and for elevated temperatures is equal to the dose rate ratio. b) Corresponding plot of **DED** data superposed to T_1 . An Arrhenius plot of the resulting shift factors is linear and yields the thermal E_a [1].

The simplest functional form of the radiative degradation rate is directly proportional to dose rate ($f(\gamma) = k^* \gamma$, k a positive constant). Gillen and Clough's proposition that a plot of **DED** versus dose rate will accurately superpose with the assumption that the degradation rate is the sum of two non-interacting processes, implies that if the thermal degradation term has Arrhenius dependence, then a radiative term directly proportional to dose rate will suffice for superposition. Thus, in this case the shift factor can be established as shown in *M1-Eq. (3)*. Note that it does not depend on the dose rate. A simple Model 1 for combined thermal and radiative degradation is summarized below:

$$r(T, \gamma) = r(T_{ref}, 0) * \exp\left(\frac{E_a}{R} \left(\frac{1}{T_{ref}} - \frac{1}{T}\right)\right) + k\gamma \quad M1 - Eq. 1$$

$$DED(T, \gamma) = \frac{C\gamma}{r(T_{ref}, 0) * \exp\left(\frac{E_a}{R} \left(\frac{1}{T_{ref}} - \frac{1}{T}\right)\right) + k\gamma} \quad M1 - Eq. 2$$

$$a_T(T) = \exp\left(\frac{E_a}{R} \left(\frac{1}{T_{ref}} - \frac{1}{T}\right)\right) \quad M1 - Eq. 3$$

Model 1: Simple radiation-thermal degradation model based on the work of Gillen and Clough with an effective degradation rate as the sum of two parallel processes (relationships *M1-Eq. 1/Eq. (2)* were implied in [1,3] but not explicitly shown). In *M1-Eq. (1)* the first term represents the thermal process, depending only on temperature. The second term represents the radiative process, depending linearly on dose rate. Note that only the thermal term has an E_a and that k is a constant with units of mol/g-Gy.

With the above definitions, it is possible to simulate and visualize Model 1 for overall rate and **DED** behavior for any temperature and dose rate conditions using *M1-Eq. (1)* and *M1-Eq. (2)*. **Fig. 2** shows simulated oxidation rate (**Fig. 2a**) and **DED** curves (**Fig. 2b**) vs. dose rate for a set of temperatures. Note that the temperature in °C is merely for convenient labeling, but for all calculations temperatures must be used in Kelvin.

For the simulations shown in **Fig. 2**, specific reference conditions and a damage equivalency had to be specified. In principle, such simulations can be obtained for any set of parameters, but we chose values that a) serve the purpose of good visualization and b) are in the range of actual properties for cable insulation materials. With this in mind, we used $T_{ref} = 28^\circ\text{C}$, $r(T_{ref}, 0) = 3.2 * 10^{-13} \text{ mol/g-s}$, $E_a = 80 \text{ kJ/mol}$, and $k = 9 * 10^{-10} \text{ mol/g-Gy}$. The latter radiative damage constant when multiplied with dose rate gives the relative radiative rate contribution. In addition, the damage is characterized by percent oxidation with $C_f = 6.25 * 10^{-4} \text{ mol/g}$ (corresponding to 2% oxidation). The same definition of C_f was used for producing all remaining plots that require its specification. It should be noted that the same horizontal dose rate superposition may be done for a plot of the oxidation rate expressed in units of mol/g-Gy (later referred to as oxidation rate per dose rate), which is simply the oxidation rate in mol/g-s divided by the respective dose rate. The superposition performed on these plots will yield the same thermal E_a . This is because the **DED** and an oxidation level per dose are inverses of each other as shown below. In some cases this analysis is more straightforward because one does not need to specify a particular failure or degradation state **C**. The plot of oxidation rate per dose rate for the above simulation is shown below as **Fig. 2c**.

$$DED(T, \gamma) = \frac{C}{r(T, \gamma)/\gamma} \quad \text{and} \quad \frac{r(T, \gamma)}{\gamma} = \frac{C}{DED(T, \gamma)}$$

Fig. 3 is an Arrhenius plot of the underlying shift factors that were obtained through superposition at an isodose of 10^4 Gy (dotted line shown on **Fig. 2b**), or alternatively through superposition of the data shown in **Fig. 2c**. The plot is linear, indicating that data following these trends will superpose in the expected Arrhenius manner, allowing for the extraction of E_a . In fact, this plot has a slope corresponding to 80 kJ/mol , precisely the E_a parameter that was used for the model simulation. Within the expectations from Model 1, we observe that at high dose rates, the **DED** curves level off (**Fig. 2b**). Since all curves approach a **DED** value of $C_f/k = 6.94 * 10^5 \text{ Gy}$ and the value of C_f is known, the value of k is easily calculated to be $9 * 10^{-10} \text{ mol/g-Gy}$, again consistent with the input parameter.

3.3. Empirical degradation rate - DED model with additional temperature dependence for radiative term

A broader empirical model for combined thermal and radiative aging was introduced by Burnay in 1990 [49] (based on the original work by Rudd [64]) as an approach towards a temperature and dose rate dependent shift factor, with some justifications for the derivations of this model, mostly as being successful for a number of materials where small temperature contributions prevented convergence at high dose rates. The first time this equation was mentioned it very likely contained two typographical errors for the E_a 's or a reversal of the notation for T_{ref} and T (*Eq. (2)* of [49]), since its thermal-only term with a 'negative E_a ' will predict a decreasing shift factor with increasing temperature, which is opposite to the logic of an accelerated degradation rate at higher temperature. Further, the radiative term (dose rate dependent second term in *Eq. (2)* in [49]) will predict the isothermal curves to diverge with increasing dose rate, which is also counter to the plot of $a_T(T, \gamma)$ vs. dose rate that was presented as **Fig. 2** in [49]. Later, these typos are neither apparent in the first IEC guidance document [65], nor in the most recent updated version ([66], p 13) which also cites Burnay's work [49], but where the shift factor equation is correctly given as below. This *Eq. (3)* leads to an alternative Model 2 describing the degradation rate and **DED** as functions of dose rate and temperature for combined radiation thermal conditions. Note that *M2-Eq. (3)* for the shift factors is simply the expanded form of *Eq. (3)* and that the symbols in *Eq. (3)* have been altered to adopt the notations used earlier in our current study.

$$a_T(T, \gamma) = \exp\left(\frac{E_a}{R}\left(\frac{1}{T_{ref}} - \frac{1}{T}\right)\right) \left[1 + k\gamma^x \exp\left(\frac{-E_a x}{R}\left(\frac{1}{T_{ref}} - \frac{1}{T}\right)\right)\right] \quad (3)$$

dose rates at any chosen isodose value. The value $\text{DED}(T_{ref}, \gamma_{ref})$ represents the particular isodose chosen. If T_i is one of the elevated temperatures and γ_{Ti} is the specific dose rate for that temperature data set that gives the same isodose value, then the a_{Ti} shift factor is given by the relevant dose rate ratio. The expression for the shift factor in terms of temperature is derived below, where the DED

$$r(T, \gamma) = r(T_{ref}, 0) * \left[\exp\left(\frac{E_a}{R}\left(\frac{1}{T_{ref}} - \frac{1}{T}\right)\right) + k\gamma^x \exp\left(\frac{E_a(1-x)}{R}\left(\frac{1}{T_{ref}} - \frac{1}{T}\right)\right) \right] \quad \text{M2 – Eq. 1}$$

$$\text{DED}(T, \gamma) = \frac{C\gamma}{r(T_{ref}, 0) * \left[\exp\left(\frac{E_a}{R}\left(\frac{1}{T_{ref}} - \frac{1}{T}\right)\right) + k\gamma^x \exp\left(\frac{E_a(1-x)}{R}\left(\frac{1}{T_{ref}} - \frac{1}{T}\right)\right) \right]} \quad \text{M2 – Eq. 2}$$

$$a_T(T, \gamma) = \exp\left(\frac{E_a}{R}\left(\frac{1}{T_{ref}} - \frac{1}{T}\right)\right) + k\gamma^x \exp\left(\frac{E_a(1-x)}{R}\left(\frac{1}{T_{ref}} - \frac{1}{T}\right)\right) \quad \text{M2 – Eq. 3}$$

Model 2: A broader empirical radiation-thermal degradation model based on the work of Burnay and Rudd with an effective degradation rate as the sum of two independent parallel processes with temperature and dose rate (M2-Eq. (3) was first published in [49]). Both the thermal and radiative terms have independent temperature dependence with individual E_a 's, but as was pointed out the E_a for the radiation component is usually low (i.e. x is close to 1).

Interestingly, it was experimentally established [49] that for the majority of elastomers x equals one, and hence the model reduces to Model 1, meaning full convergence of data at high dose rates. For practical purposes of data analysis, M2-Eq. (2) is fitted to temperature-dose rate data in two separate steps. The activation energy parameter E_a is determined from thermal-only data [49]. Data at different dose rates all taken at the reference temperature T_{ref} are used to fit the values of the parameters k and x . Note that these two analysis steps are independent, which implies that Model 2 also assumes no synergism between the thermal and radiative contributions to the overall oxidation/degradation rate, but indirectly can accommodate increasing synergism through the radiative E_a (see section 7). Further, an exponent of less than one for the dose rate describes a likely decrease in the ‘oxidative effectiveness’ of the irradiation for some materials as the dose rate increases. While x is an empirical parameter, it allows for the radiative oxidation rate to diverge from being fully proportional to dose rate. This accommodates an increasing ‘inert’ irradiation response, hence covers a subtle change in degradation chemistry with inert crosslinking beginning to contribute at higher dose rates. The exponent compensates somewhat for the radiative E_a (which increases the radiative rate) and thereby finely tunes the description of the material behavior at higher dose rates. A more detailed description of the analysis process can be found in [66] which explains the process of data analysis utilizing superposition of either material damage (i.e. elongation or compression set) versus time, or dose (DED) versus dose rate data.

It is important to now recognize, that for any model that contains a temperature-dependence in the radiative term, it is not possible to obtain the underlying thermal E_a using traditional t-T-r or DED data superposition shown in Fig. 1a. If a comprehensive data set for DED with temperature is available, then Burnay's model could be globally fitted using M2-Eq. (2) to yield the underlying thermal E_a and additional model parameters. In contrast, a generic isodose superposition (horizontal shifting along the dose-rate axis) can only approximate the underlying thermal E_a , due to the radiative rate that is in itself temperature dependent. From Fig. 1 it is apparent that the shift factors a_T are proportional to the ratios of

(isodose) value at an elevated temperature and dose rate must equal the DED value at the reference condition. This implies that the DED shifting procedure for kinetic models that contain more complex functional terms for the radiative rate contribution will yield good approximations of the shift factors when the shifting procedure is accomplished at low dose rates. For practical purposes usually dose rates lower than 10 Gy/h at moderate temperatures reveal the temperature shift factors for materials of interest.

$$t_i = \text{DED}/\gamma_{Ti} \quad t_{ref} = \text{DED}/\gamma_{Tref}$$

$$\text{DED}(T_i, \gamma_{Ti}) = \text{DED}(T_{ref}, \gamma_{Tref})$$

$$\Rightarrow \frac{C\gamma_{Ti}}{r(T_{ref}, 0) * \exp\left(\frac{E_a}{R}\left(\frac{1}{T_{ref}} - \frac{1}{T_i}\right)\right) + f(\gamma_{Ti})} = \frac{C\gamma_{Tref}}{r(T_{ref}, 0) + f(\gamma_{Tref})}$$

$$\Rightarrow \frac{\gamma_{Ti}}{\gamma_{Tref}} = \frac{t_{ref}}{t_i} = \frac{r(T_{ref}, 0) * \exp\left(\frac{E_a}{R}\left(\frac{1}{T_{ref}} - \frac{1}{T_i}\right)\right) + f(\gamma_{Ti})}{r(T_{ref}, 0) + f(\gamma_{Tref})}$$

$$\Rightarrow \lim_{\gamma_{Ti}, \gamma_{Tref} \rightarrow 0} \frac{\gamma_{Ti}}{\gamma_{Tref}} \rightarrow \exp\left(\frac{E_a}{R}\left(\frac{1}{T_{ref}} - \frac{1}{T_i}\right)\right) = a_{Ti}$$

Using M2-Eq. (1) and M2-Eq. (2) for an overview of the model features, it is now possible to simulate as before oxidation rates (Fig. 4a) and DED curves (Fig. 4b) for different temperature conditions using similar material property definitions with $T_{ref} = 28^\circ\text{C}$, $r(T_{ref}, 0) = 3.2 * 10^{-13} \text{ mol/g-s}$, $E_a = 80 \text{ kJ/mol}$, $k = 2.8 * 10^3 \text{ s}^x/\text{Gy}^x$, and $x = 0.9$. We include a plot of oxidation rates per dose rate for the above simulation as Fig. 4c. Most importantly, we observe in all figures that the curves do not converge for high dose rates. Thus, Model 2 will be more appropriate in describing experimental data that do not show perfect convergence to a single damage level at high dose rates as was shown for a few materials [49]. A superposition below the limiting value of $6.94 * 10^5 \text{ Gy}$ will yield an

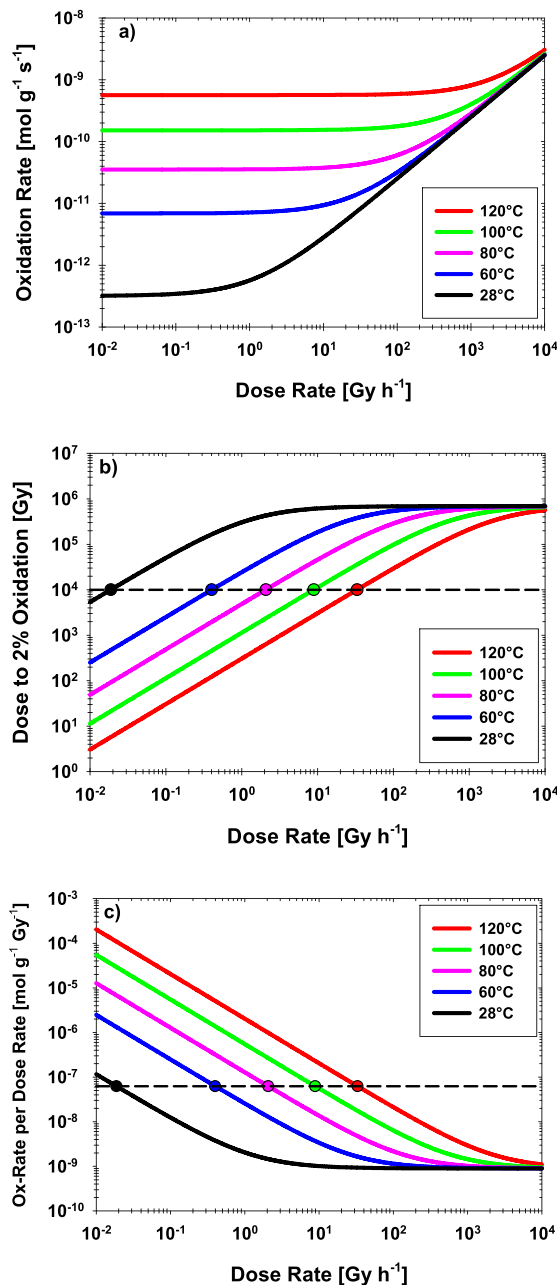


Fig. 2. a) Simulated oxidation rates for a basic radiation-thermal degradation model with an effective degradation rate as the sum of two independent parallel processes (Model 1). The rate is characterized by a thermal E_a of 80 kJ/mol and referenced to 28 °C. b) Simulated DED vs. dose rate curves. c) Simulated oxidation rates expressed per dose rate. All curves in these plots converge at high dose rates.

approximate value for the thermal E_a , but cannot be precise because of the contribution of the secondary radiative term.

For the discussion here, it is important to recognize that Model 2 includes Model 1 as a subset solution, and hence experimental data that fit Model 1 will equally fit Model 2 without any need for adjustments in the high dose rate regime. However, Model 2 through the incorporation of an additional ‘degree of freedom’ has been the first attempt to describe higher dose rate aging behavior that may show subtle temperature dependence on its own. The origin of such behavior is open to further discussion, subject to uncertainty in data, the acquisition of more comprehensive data sets, and the question whether radiation initiated degradation should perhaps

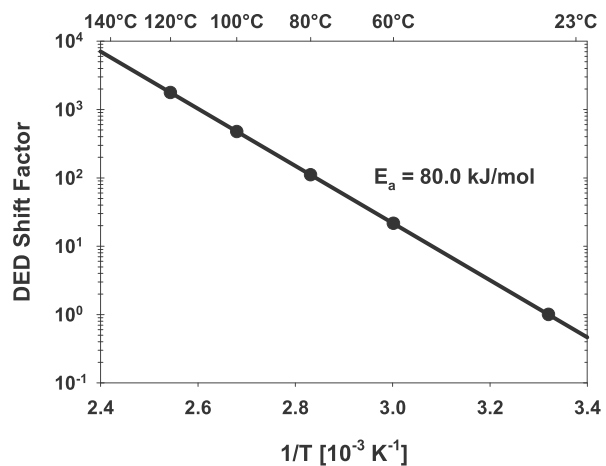


Fig. 3. Arrhenius plot of the resulting shift factors when horizontally superposing the curves in Fig. 2b at a DED (isodose) value of 10⁴ Gy yielding the underlying thermal E_a of 80 kJ/mol (equivalent to model input). A similar dose rate superposition at any isodose value below the limiting value (here 6.94 × 10⁵ Gy) will yield the same E_a . A corresponding superposition can also be accomplished when oxidation rates are given in mol/g-Gy (see Fig. 2c) above the limiting rate of 9 × 10⁻¹⁰ mol/g-Gy.

show a small temperature dependence as we discussed in the introduction (follow-up chemistry and molecular mobility aspects that depend on temperature as was shown for UV degradation). For the description of combined degradation behavior, Model 2 is certainly more comprehensive than Model 1, and as a step forward can accommodate subtle and perhaps unexpected data divergence in the high dose rate regime. We do not suggest that actual aging data must necessarily follow Model 2, we just wish to point out that appropriate model descriptions can be derived as needed or even simplified as shown later.

3.4. Superposition of DED or degradation rates to yield E_a

At this point it is important to recognize that accelerated aging is sometimes conducted to yield degradation rate parameters rather than DED data that define damage for particular exposure conditions. While it is clear that available DED data can be easily shifted to yield the thermal E_a for Model 1, the situation is more complicated if only degradation rates are available, or if the radiative rate has an additional temperature dependence (such as in Model 2). If oxidation rates are experimentally available and follow similar trends as shown in Figs. 2b and 4b, they could then be fitted to either M1-Eq. (1) or M2-Eq. (1) to yield the thermal E_a . One intuitive alternative may be the use of a traditional Arrhenius plot of degradation rate vs. inverse temperature using degradation rate data all obtained at a single dose rate, but at different temperatures. Importantly, such an approach will not yield linear Arrhenius behavior and could lead to miss-interpretation of aging data or doubtful extrapolations except for sufficiently low dose rates, where the thermal process will represent the underlying Arrhenius behavior. The Arrhenius plots of oxidation rate vs. inverse temperature will have curvature as long as the aging has contributions from the radiative term. This situation is illustrated below in Fig. 5, which shows Arrhenius plots generated from the modeled rate data in Fig. 2a (M1-Eq. (1)), and in Fig. 6 obtained from the modeled rate data in Fig. 4a (M2-Eq. (1)), with all the relevant model parameters mentioned previously.

The exact thermal E_a can only be obtained from the thermal-only data, where the radiative term is truly irrelevant, for example if one uses aging rate data for high temperature and low

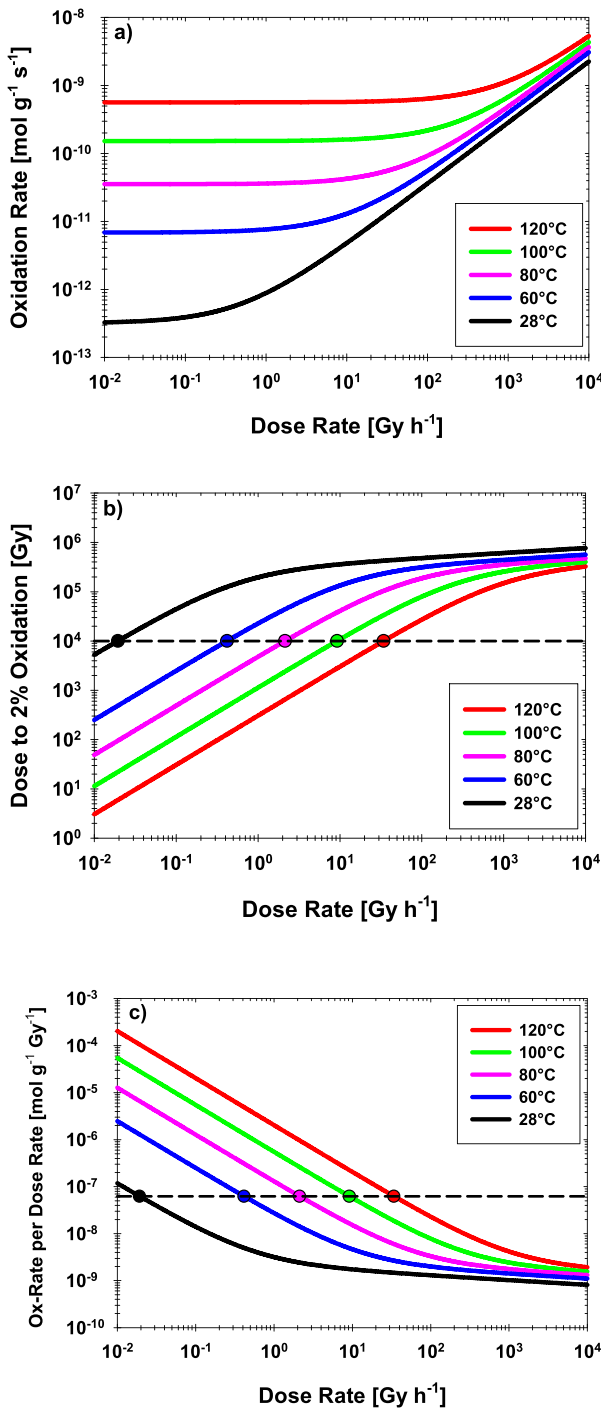


Fig. 4. a) Simulated oxidation rates for a more complex combined radiation-thermal degradation model given as Model 2 [49] with the two key features of a thermal component (E_a of 80 kJ/mol referenced to 28 °C) and a radiative component as comprised of two factors (the first factor proportional to a power of the dose rate (here 0.9), and the second factor having a small Arrhenius dependence on temperature (here 8 kJ/mol)). b) Simulated DED vs. dose rate curves for Model 2. c) Simulated oxidation rates per dose rate for Model 2. The curves do not converge at high dose rates, but approach equal slopes on the log-log plots defined by the exponent for dose rate.

dose rate conditions. In comparison, even at low temperatures and low dose rates the combined aging rate data cannot be used for the determination of the underlying thermal E_a . Individual curved Arrhenius behavior results for such data, which without a theoretical understanding and the availability of a suitable aging model,

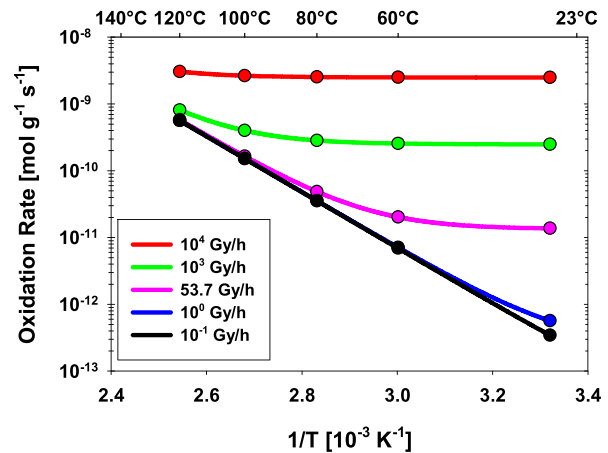


Fig. 5. Arrhenius plots generated using Model 1 with a T_{ref} of 28 °C and thermal E_a of 80 kJ/mol. Note that the lowest dose rate approaches the thermal boundary while the highest dose rate approaches the expected zero E_a under radiation dominant conditions. For intermediate dose rates, the Arrhenius plots show varying curvature. The most nonlinear Arrhenius plot here exists at a dose rate of about 54 Gy/h. Hence, the use of such Arrhenius plots for determining the thermal E_a is justifiable only at very low dose rates.

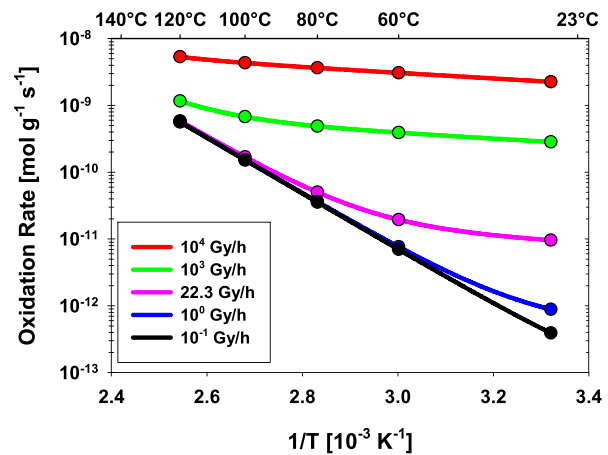


Fig. 6. Arrhenius plots generated using Model 2 with a T_{ref} of 28 °C, thermal E_a of 80 kJ/mol, and $\alpha = 0.9$. Note, that as in Fig. 5 the Arrhenius plot is nearly linear at the lowest dose rate and allows for an appropriate thermal E_a to be determined. The most nonlinear Arrhenius plot here occurs at a dose rate of about 22 Gy/h. The high dose rate plot reaches the boundary of the radiative E_a (here 8 kJ/mol).

makes it impossible to derive extrapolation for predictive purposes towards low dose rate-temperature conditions.

For any model of degradation rate of the form $r(T, \gamma) = g(T, \gamma) * \exp\left(\frac{E_a}{R} \left(\frac{1}{T_{ref}} - \frac{1}{T}\right)\right)$ with g having any form other than $g = \exp(b/T)$ and b a constant, an Arrhenius plot of rate vs. inverse temperature will always exhibit curvature. The reason is that for the Arrhenius plot to be linear in principle, the following condition must be met:

$$\frac{d^2 \ln(r(T, \gamma))}{d(1/T)^2} = 0 \text{ for all } r(T, \gamma) \text{ in the domain of interest.}$$

This implies that g must satisfy, with γ fixed, the differential equation

$$\frac{d^2g(1/T)}{d(1/T)^2} - \frac{1}{g\left(\frac{1}{T}\right)} \left(\frac{dg\left(\frac{1}{T}\right)}{d\left(\frac{1}{T}\right)} \right)^2 = 0$$

the general solution of which is $c_1 \exp(c_2/T)$ where c_1 and c_2 do not depend on temperature. For example, $g(T, \gamma) = \gamma$ would allow for linear Arrhenius behavior (in this case $c_1 = \gamma$ and $c_2 = 0$), but not $g(T, \gamma) = \gamma + \exp\left(\frac{-E_a}{R}\left(\frac{1}{T_{ref}} - \frac{1}{T}\right)\right)$ because there are no c_1, c_2 that satisfy this function. This is important to remember if primary data are oxidation rates at different temperatures and dose rate conditions because in this case, if the underlying degradation model is anything more complicated than just an Arrhenius relationship with temperature, it will be necessary to do either of the following.

3.5. Enhanced degradation rate – DED model with independent E_a 's for thermal and radiative components

As discussed above, an attractive feature of any aging model is to easily yield the underlying activation energy based on data superposition. If aging data do not superpose then the determination of any E_a for predictive purposes is challenging. It may well be that a different model for the rate, **DED** or shift factor conditions better describes a material data set, but it may not allow for easy data superposition. Building on the concept introduced by Burnay of a second E_a for the radiation domain [49], the simplest model with two independent E_a 's is given below. In this Model 3, k is a constant, E_1 is the thermal activation energy, and E_2 is called the radiative activation energy. The addition of an E_a for the radiative term provides a further degree of freedom with a stronger impact in the high dose-rate regime, but as will be shown in section 7, such behavior for high dose-rates can also be consistent with synergistic effects.

$$r(T, \gamma) = r(T_{ref}, 0) * \exp\left(\frac{E_1}{R}\left(\frac{1}{T_{ref}} - \frac{1}{T}\right)\right) + k\gamma \exp\left(\frac{E_2}{R}\left(\frac{1}{T_{ref}} - \frac{1}{T}\right)\right) \quad M3 - Eq. 1$$

$$DED(T, \gamma) = \frac{C\gamma}{r(T_{ref}, 0) * \exp\left(\frac{E_1}{R}\left(\frac{1}{T_{ref}} - \frac{1}{T}\right)\right) + k\gamma \exp\left(\frac{E_2}{R}\left(\frac{1}{T_{ref}} - \frac{1}{T}\right)\right)} \quad M3 - Eq. 2$$

Model 3: Radiation-thermal degradation model with an effective degradation rate as the sum of two independent parallel processes with temperature and dose rate. Both the thermal and radiative term have individual E_a . There is no straightforward form for a shift factor because as demonstrated below, there is no perfect superposition for **DED** curves following this model.

1. Use the primary data to produce a different plot (e.g. **DED** or oxidation rates in mol/g-Gy vs. dose rate) that will allow for superposition to determine the thermal E_a , after which any other parameters may be extracted. This was demonstrated for Model 1 and Model 2.
2. Use a different method not involving superposition that allows for the determination of the model parameters, e.g. a global multivariable curve fit, which is attractive when the degradation model is more complex. Examples are shown in Section 4.

The challenge is how to conduct appropriate accelerated aging experiments and suitable data interpretation. Suppose one conducts simple experiments at a range of temperatures and at fixed dose rate in analogy with the usual approach of just varying temperature for traditional accelerated thermal aging. Then the resulting Arrhenius analysis may be seen as yielding some average E_a within the scatter of the data. However, unless an aging model with the overall theoretical framework is considered, then this E_a and the available data have no value for any predictive purposes at other dose rates. This emphasizes that combined radiation-thermal oxidative aging of polymer materials cannot be simplified, and only comprehensive aging tests can truly provide the insight for overall material behavior. Further, the usual kinetic analysis of degradation rates in the time domain (mol/g-s) and their Arrhenius interpretation does not relate to data shifting and superposition within the dose rate space. This can only be accomplished if rates are converted into mol/g-Gy where shifting along dose rates will then yield the thermal E_a .

With this definition, simulated oxidation rates (*M3-Eq. (1)*) and **DED** curves (*M3-Eq. (2)*) can be generated, as shown in Fig. 7a and Fig. 7b, respectively, for the following parameters: $r(T_{ref}, 0) = 3.2 * 10^{-13}$ mol/g-s, $k = 9 * 10^{-10}$ mol/g-Gy, $E_1 = 80$ kJ/mol, $E_2 = 15$ kJ/mol, and $T_{ref} = 28$ °C.

The **DED** vs. dose rate plots show similar behavior as shown before for Model 2 in that the curves do not converge to the same damage level at high dose rates. However, the difference between the two approaches is obvious. Model 3 results in parallel **DED** levels at high dose rates, whereas Model 2 forces a slope in the **DED** vs. dose rate behavior for high dose rates which has been shown to be equal to $(1-x)$ [66]. This clearly shows the influence of the empirical factor in Model 2. As a consequence, the Arrhenius plots for Model 3 in Fig. 8 do not have the same slope at different isodose conditions. For these **DED** curves to fully superpose, an Arrhenius plot at any possible isodose condition should exhibit a single slope, characteristic of the thermal E_a . This confirms that the horizontal dose rate superposition is not legitimate for extracting the thermal E_a . Further, curves of oxidation rates per dose rate cannot be superposed either. The best fit E_a for the shift factors at isodose 10^5 Gy is ~87.3 kJ/mol, while at isodose 10^4 Gy it is ~80.5 kJ/mol. This shows the influence of the combination of the two E_a 's and the fact that the thermal E_a exists as a boundary for low isodose data. For combined high isodose and high dose rates the local E_a will be the sum of the two E_a 's.

We note the similarity between Model 2 and Model 3. Specifically, Model 2 exhibits a 'radiative activation energy' similar to E_2 in Model 3, except that it is given by $E_a(1-x)$. We also recognize that in Model 2, the radiative term contains a factor of the dose rate raised to the power x , while in Model 3, the power of the dose rate

is one. That is, Model 2 does not allow the radiative E_a term and the power of the dose rate to vary independently, as it does in Model 3. With the above considerations we wish to introduce a modified theoretical model that allows the power of the dose rate to be varied. This is shown as Model 4 below, which has two independent E_a 's (as the basic Model 3) and an additional empirical adjustable parameter, similar to the feature of Burnay's original approach [49].

This model is also similar to that proposed by Ito [50–52], and we believe that this offers sufficient degrees of freedom to fit any data set involving constant oxidation rates, constant synergism contributions, and consistent time behavior in mechanical property changes (see section 6), yet cannot address inverse temperature or DLO behavior [13,32,33].

$$r(T, \gamma) = r(T_{ref}, 0) * \exp\left(\frac{E_1}{R}\left(\frac{1}{T_{ref}} - \frac{1}{T}\right)\right) + k\gamma^x \exp\left(\frac{E_2}{R}\left(\frac{1}{T_{ref}} - \frac{1}{T}\right)\right) \quad M4 - Eq. 1$$

$$DED(T, \gamma) = \frac{C\gamma}{r(T_{ref}, 0) * \exp\left(\frac{E_1}{R}\left(\frac{1}{T_{ref}} - \frac{1}{T}\right)\right) + k\gamma^x \exp\left(\frac{E_2}{R}\left(\frac{1}{T_{ref}} - \frac{1}{T}\right)\right)} \quad M4 - Eq. 2$$

Model 4: Improved empirical radiation-thermal degradation model with an effective degradation rate as the sum of two independent parallel processes with temperature and dose rate, with the power of the dose rate as an additional empirical model parameter. With this additional degree of freedom, this model may enable a better fit to oxidation rate and related DED data. Again, note that a shift factor is not included because perfect DED superposition is not possible for DED curves following this model.

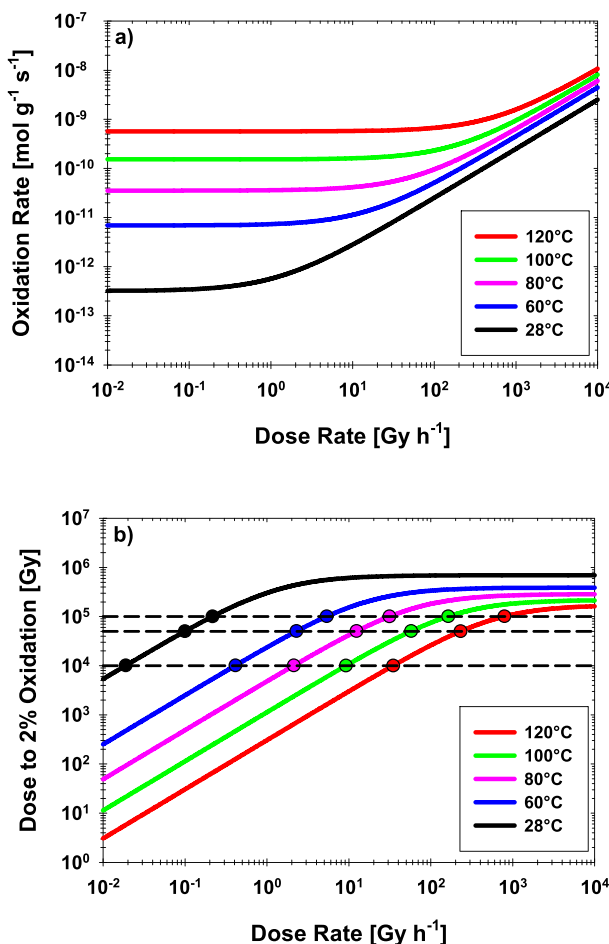


Fig. 7. a) Simulated oxidation rate curves for Model 3. The plots have a T_{ref} of 28 °C, a thermal E_a of 80 kJ/mol, and a radiative E_a of 15 kJ/mol b) Simulated DED vs. dose rate curves for Model 3. Note that the curves do not converge for high dose rates, but approach identical slopes, similar to Model 2.

We simulate oxidation rates (M4-Eq. (1), Fig. 9a) and DED curves (M4-Eq. (2), Fig. 9b) using the same parameters as before with $k = 9*10^{-10}$ mol*s^{x-1}/g-Gy^x, and in addition $x = 0.9$. Fig. 10 shows the Arrhenius plot of the shift factors obtained by superposing the DED curves at three different isodose values. As was seen for Model 3, Model 4 also does not allow for the extraction of the thermal E_a from the horizontal dose rate superposition as evidenced by these diverging Arrhenius plots. At isodose 10^5 Gy the best fit E_a is 86.7 kJ/mol, while at isodose 10^4 Gy it is 80.5 kJ/mol. Again, this demonstrates the interaction between the two E_a 's and the thermal boundary given by low isodose/dose rate data analysis. We now turn to the second approach mentioned earlier: the use of a global multivariable curve fit to oxidation rate data to determine underlying model parameters.

4. Oxidation rates analyses with four different models

We used MATLAB® to perform global curve fits of our oxidation rate data to the different models (M1-Eq. (1) to M4-Eq. (1)) by utilizing and minimizing the objective function (sum of squares of normalized residuals, $SSNR$) given in Eq. (4).

$$SSNR = \sum_i \sum_j \left(\frac{\hat{r}(T_j, \gamma_i) - r(T_j, \gamma_i)}{\hat{r}(T_j, \gamma_i)} \right)^2 \quad (4)$$

Here, \hat{r} indicates a measured rate and r indicates the modeled rate at the same temperature and dose rate. As an example, overview experimental oxidation rate data for the Eaton Dekoron Hypalon jacket material exposed in the LICA facility were fitted to M1-Eq. (1) under the minimization conditions given by Eq. (4) as shown in Fig. 11. The fit yields the following values for the model parameters with $T_{ref} = 28$ °C fixed: $r(T_{ref}, 0) = 1.02*10^{-13}$ mol/g-s, $E_a = 76.6$ kJ/mol, and $k = 1.13*10^{-9}$ mol/g-Gy. The fit returned an $SSNR$ of 5.97. We notice that the fit is especially poor for the data at the highest temperatures and highest dose rates. Moreover, the data seem to suggest that the rates do not converge for high dose rates, but rather appear to stay apart and have additional subtle temperature

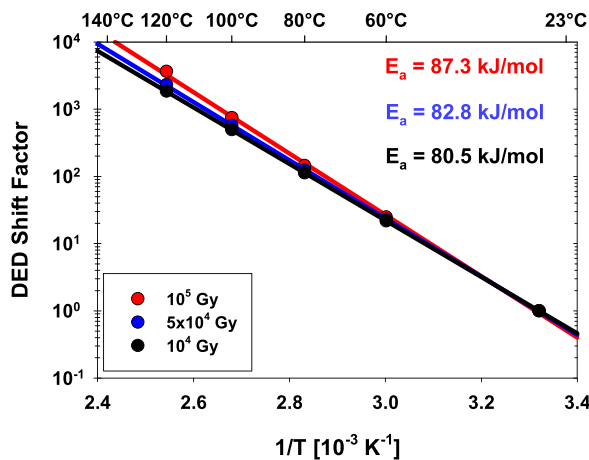


Fig. 8. Shift factors vs. inverse temperature obtained when superposing the curves in Fig. 7b at different isodose values (10^4 – 10^6 Gy) using Model 3. Note that the three Arrhenius plots diverge at high dose levels implying that the usual **DED** dose rate superposition is no longer valid.

dependence. As discussed later such a behavior would also be consistent with synergistic effects.

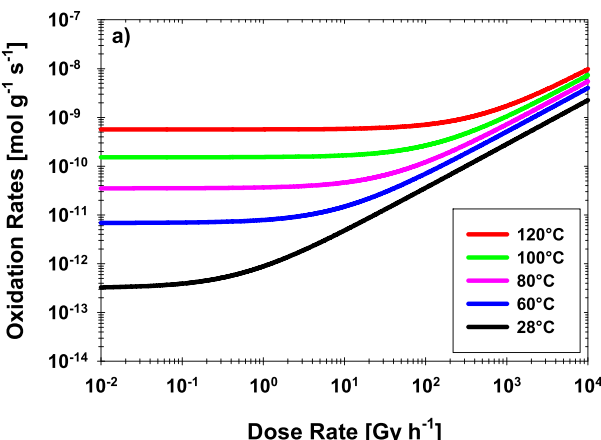


Fig. 9. a) Simulated oxidation rate curves for Model 4. The plots have a T_{ref} of 28 °C, a thermal E_a of 80 kJ/mol, a radiative E_a of 15 kJ/mol, and $\alpha = 0.9$. b) Simulated **DED** vs. dose rate curves for Model 4. Again the curves do not converge for high dose rates, but approach identical slopes.

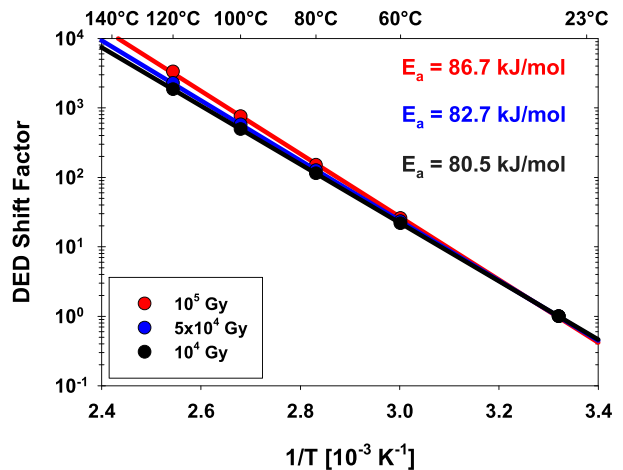


Fig. 10. Plot of shift factors vs. inverse temperature obtained when superposing the curves in Fig. 9 at different isodose values (10^4 – 10^6 Gy) for Model 4. Again, the three Arrhenius plots diverge at high dose levels demonstrating that the usual **DED** dose rate superposition is no longer valid.

The data were also fitted to Model 2 (M2-Eq. (1)) with $T_{ref} = 28$ °C fixed again and using Eq. (4) as the objective function. The fit is shown in Fig. 12 and yields the following parameters with an **SSNR** of 4.22: $r(T_{ref}, \theta) = 4.44 \cdot 10^{-14}$ mol/g-s, $r(T_{ref}, \theta) \cdot k = 4.40 \cdot 10^{-10}$ mol*s⁻¹/g-Gy^x, $E_a = 85.8$ kJ/mol, and $x = 0.837$. We next fit the data to the empirical Model 3 (M3-Eq. (1)) also with $T_{ref} = 28$ °C. The fit is shown in Fig. 13 and yields the following fitted parameters with an **SSNR** of 2.85: $r(T_{ref}, \theta) = 9.85 \cdot 10^{-14}$ mol/g-s, $k = 9.18 \cdot 10^{-10}$ mol/g-Gy, $E_1 = 76.0$ kJ/mol, and $E_2 = 14.2$ kJ/mol.

We observe in Fig. 13 that the curves match the data much more closely than seen in Figs. 11 and 12. This analysis suggests the importance of allowing for two independent activation energy terms in the rate model. The next step was to fit the data to the most comprehensive, Model 4 (M4-Eq. (1)), with $T_{ref} = 28$ °C fixed. The fit yields the following values for the model parameters and is shown as Fig. 14: $r(T_{ref}, \theta) = 7.77 \cdot 10^{-14}$ mol/g-s, $k = 6.68 \cdot 10^{-10}$ mol/g-Gy, $E_1 = 78.7$ kJ/mol, $E_2 = 16.3$ kJ/mol, and $x = 0.936$. The fit returned an **SSNR** of 2.60, which is slightly better than that obtained using Model 3. It is important to see that the power is close to 1, but that the radiative activation energy E_2 is certainly much greater

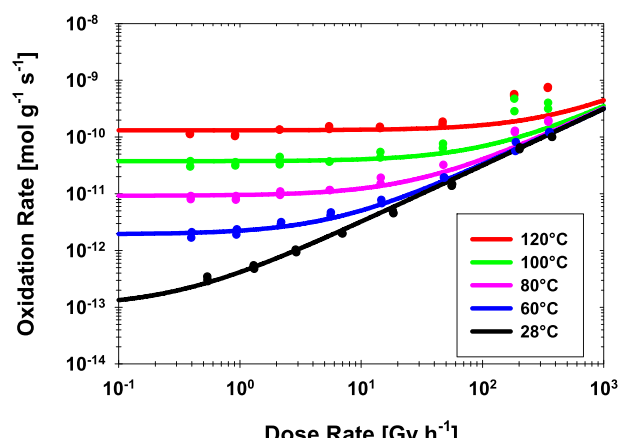


Fig. 11. Oxidation rate data for the Eaton Dekoron Hypalon cable jacketing material fitted to Model 1 (M1-Eq. (1)). The model describes the data over most of the dose rate range very well. Deviations are apparent at the highest dose rates since in this region the model curves begin to converge, while the data do not.

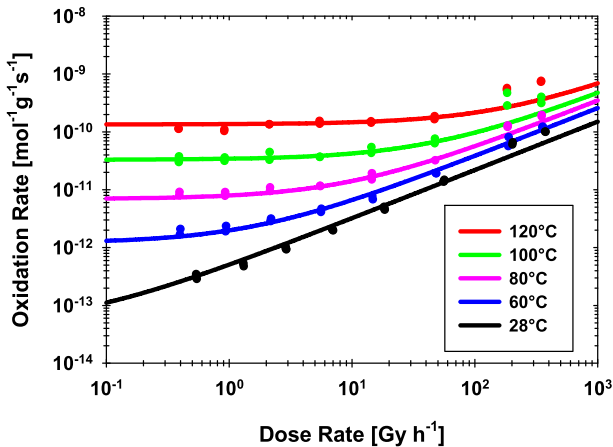


Fig. 12. Oxidation rate data for the Eaton Dekoron Hypalon jacketing material fitted to Model 2 (M2-Eq. (1)).

than zero, and on the order of what was seen before for Model 3. This seems to discourage Model 2 (M2-Eq. (1)) which would suggest that for α being close to one, the activation energy in the second (radiative) term should be very small.

Using 2% oxidation as the damage level, we can now simulate as before curves of **DED** vs. dose rate (Fig. 15) using both Model 1 (worst fit) and Model 4 (best fit) where the model parameters are precisely those acquired from the previous fits to the rates. Shown in Fig. 16 are also comparative plots of **TED** vs. dose rate generated from Models 1 and 4. We see that at low dose rates, the use of Model 1 (dashed line) shows a subtle underestimation relative to Model 4 (solid lines) of the **DED** (Fig. 15) and **TED** (Fig. 16), respectively. Similarly, we could also observe differences between Model 2 and Model 4 by simulating **DED** (Fig. 17) and **TED** (Fig. 18) versus dose rate using the same parameters given for Figs. 12 and 14, respectively. We recognize that the curves are practically identical at low dose rates, but diverge significantly for high dose rates.

5. Interpretation of thermal E_a for specific cable insulation material

A meaningful addition to combined environment aging models is intrinsic time dependence of the oxidation rate, since this is often

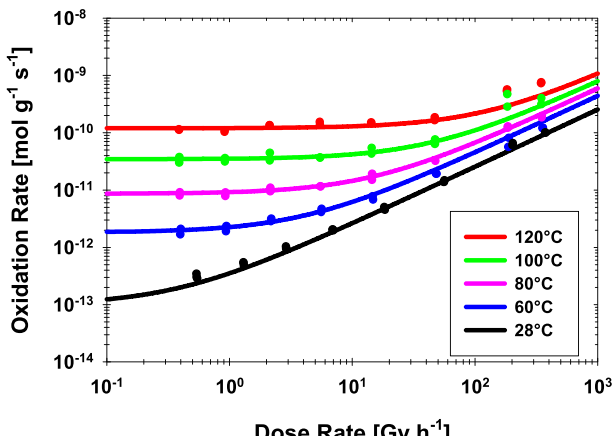


Fig. 13. Oxidation rate data for the Eaton Dekoron Hypalon jacketing material fitted to Model 3 (M3-Eq. (1)). When compared with Fig. 12, it is clear that Model 3 better describes the oxidation rate data at the highest dose rates.

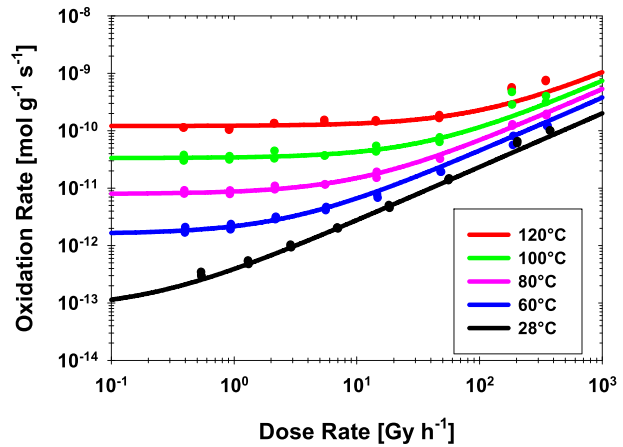


Fig. 14. Oxidation rate data for the Eaton Dekoron Hypalon jacketing material fitted to Model 4 (M4-Eq. (1)). This is the most general of the four models discussed in this paper (assuming constant oxidation rates) and yields the best fit to the data (based on residual error).

observed in actual aging data, at least for thermal degradation, as declining with time. The reader is referred to examples for oxidation rate and oxidation level behavior with time in the literature [5]. The incorporation of time dependence requires us to carefully distinguish between initial thermal degradation rates and its E_a (the initial low dose rate boundary for the aging model discussed here), and analysis of DED or similarly integrated damage state data (% oxidation or elongation at break) which will contain any embedded rate dependence with time, but will also deliver the E_a that is often quoted in the literature [5].

We begin by considering thermal-only oxidation rate data, as an example for the Eaton Dekoron Hypalon jacket material that we exposed in the LICA facility. As mentioned earlier, one ampoule per dose rate was twice aged with increasing temperature ranging from a total exposure time of 400 h at 28 °C to 46 h at 120 °C. The initial thermal-only oxidation rates for each temperature of the LICA study (28 °C, 60 °C, 80 °C, 100 °C, and 120 °C) were determined using the improved time-independent Model 4 with fitted parameters and $\gamma = 0$ (see section 4 Fig. 14), and are plotted in Fig. 19. In addition, thermal-only data were acquired in laboratory aging

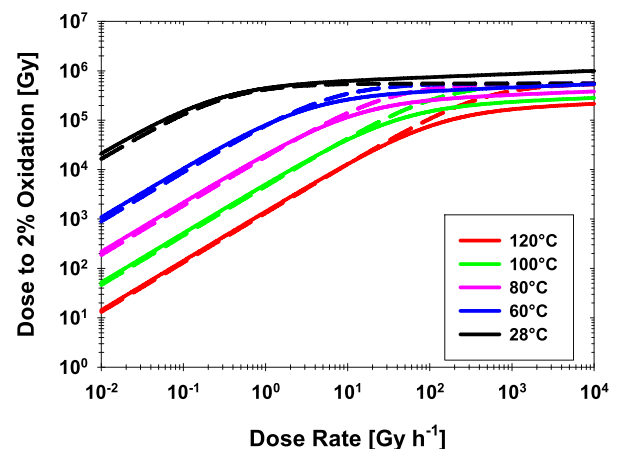


Fig. 15. Simulated **DED** curves using the fitted parameters from Model 1 (dashed lines) and Model 4 (solid lines). Note that at low dose rates, Model 1 slightly underestimates **DED** relative to Model 4. Since Model 4 yields the best fit to the oxidation rate data for the Eaton Dekoron Hypalon material, we are confident that this enables a more accurate estimate of the **DED** at low dose rates.

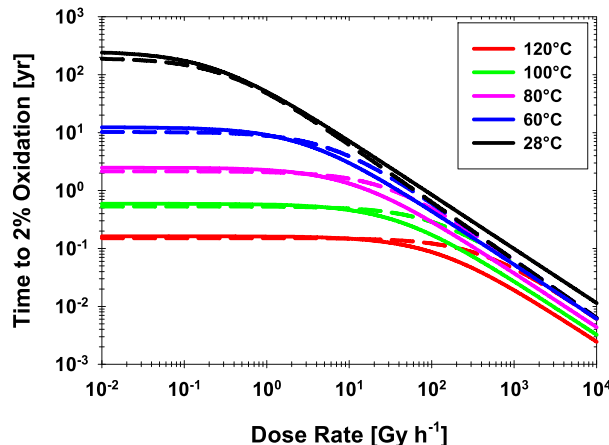


Fig. 16. Simulated **TED** curves using the fitted parameters from Model 1 (dashed lines) and Model 4 (solid lines). Note that at low dose rates, Model 1 slightly underestimates the **TED** relative to Model 4.

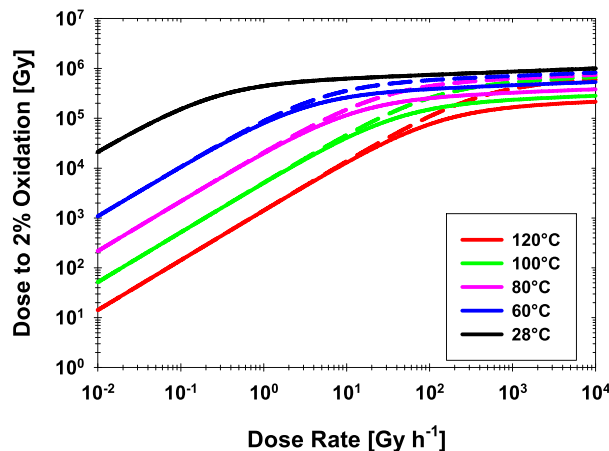


Fig. 17. Simulated **DED** curves using the fitted parameters from Model 2 (dashed lines) and Model 4 (solid lines). The curves are identical at low dose rates. The model curves only differ noticeably for dose rates greater than about 1 Gy/h.

ovens for new samples each at 23 °C, 50 °C, 80 °C, and 110 °C (also shown in Fig. 19), again with the intent of only obtaining early rates and not conducting a comprehensive investigation into its time-dependence as aging levels evolve. There is good agreement between the thermal-only data measured in laboratory aging ovens and the predicted boundary values from the LICA study, which of course supports the thermal boundary concept in the radiation-thermal model. The two Arrhenius plots yield a thermal E_a for the initial rates of ~79 kJ/mol.

A single representative thermal E_a for thermal-only aging is an expected material property, regardless of the method used to determine this value or the type of aging data analyzed. This means the thermal E_a should match those obtained from oxidation rates, or integrated as extent of oxidation, or **DED** data that may originate from mechanical property changes, as long as given oxidation levels relate to equal mechanical degradation states independent of temperature (see earlier definition of C_f in section 3.1).

Unfortunately, the initial degradation rates in thermal aging studies are not always emphasized and quoted. Instead, cumulative degradation levels, either as % oxidation or elongation at break, are usually examined with time-temperature superposition and its corresponding E_a reported [14,37,67]. This requires us to highlight

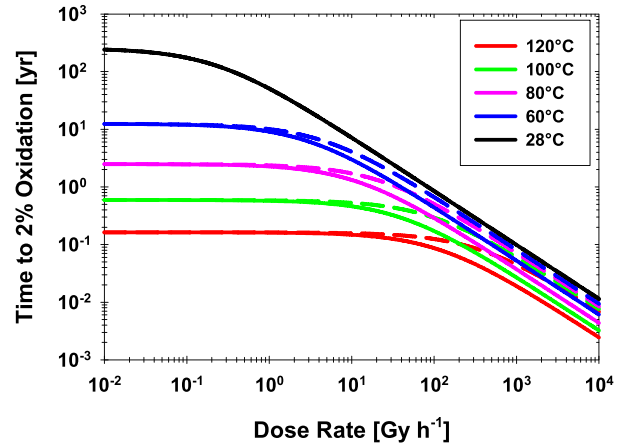


Fig. 18. Simulated **TED** curves using the fitted parameters from Model 2 (dashed lines) and Model 4 (solid lines). The curves are identical at low dose rates. The model curves only differ substantially for dose rates greater than ~10 Gy/h. For the purpose of modeling combined thermal radiative aging of cable insulation materials, the resulting estimation of material lifetimes for low dose rates will be nearly identical for Model 2 or Model 4.

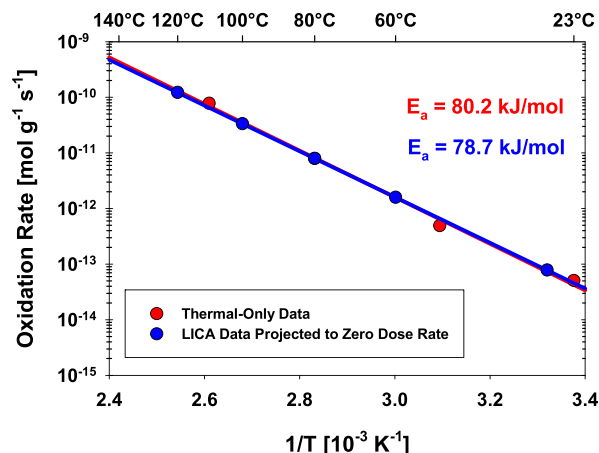


Fig. 19. Plots of oxidation rate data collected for the Eaton Dekoron Hypalon jacket material. Data were obtained for a range of dose rates (see Fig. 11) and projected to zero dose rate using Model 4. Additional data were obtained from aging individual fresh samples in aging ovens. Both experiments yield near identical linear Arrhenius behavior with a thermal E_a for initial rates of ~79 kJ/mol.

potential differences in the determination of a thermal E_a . A complication occurs when the thermal oxidation rate is significantly time-dependent over the time-frame where material aging and mechanical property changes are measured. Aging data acquired in this manner will have the underlying time dependence embedded when performing time-temperature superposition analysis of oxidation levels versus time, and will yield a different value for a thermal E_a than obtained from initial rates. For example, a higher thermal E_a of 90.7 kJ/mol is obtained from all shift factors for oxidation levels published for a similar Samuel Moore Dekoron Hypalon jacket material (see a_T values in Figure IV-17 [5]). While the E_a obtained from such an analysis of integrated oxidation, mechanical property changes or similar **DED** data often serves its purpose for performance predictions, it may not be equated with an E_a for initial degradation rates. Instead, it should be discussed as an E_a for material oxidation/damage accumulation rates, of course having its own merit for relevant interpretation and use. We will

hence illustrate this situation with a simple ‘idealized’ behavior to emphasize the nature of time-dependency in thermal aging.

5.1. Time dependence for oxidation/degradation rate

Time-dependent degradation rates are often embedded in cumulative aging data (e.g. **DED** superposition for elongation, or cumulative oxidation) and the resulting E_a will therefore not match that of the initial rates. We wish to demonstrate this for a situation where the oxidation rate follows a power law relationship with cumulative aging time and focus on thermal only conditions to provide a simple illustrative example. There is no explicit expectation that a material must follow this behavior. When thermally aged many materials display near constant oxidation rates with time [34–38,60,68,69], but a power law dependence for thermal aging of PMDI foam, Nylon [70], and other elastomers has also been observed [5]. Further, the experimental observation of excellent superposability at all aging states with deviation from unity in the slope of a log-log plot implies that such power laws with time apply, despite our intuition that perhaps only reaching a specific oxidation/degradation level should trigger a declining rate. Time-dependence of oxidation rates is an outstanding and poorly understood issue in polymer degradation. We would expect rates to depend on absolute oxidation levels and not rates to simply evolve with time. Further, with time-dependence the true initial condition also becomes rather elusive. We also do not know if rates have a tendency to initially decline and then perhaps level off or how long the declining behaviors occurs at different temperatures. Further, we don't know if only the thermal rate, the radiative rate or their combination follow similar time dependence. Hence, our emphasis is to point out that time-dependence in oxidation rates can be a convoluting behavior, and would have to be defined and dealt with for different circumstances in any aging model.

An example is given for Model 4 which includes a declining oxidation rate following a power law as defined in Eq. (5), where α is a constant and time t is the cumulative aging time for the material. Time t_0 is an initial aging time small enough so that the material aged at the conditions T and γ for time t_0 may still be considered unaged. In addition, we will assume that $t_0 \ll t_1$ where t_1 is the cumulative aging time corresponding to the first rate measurement. Eq. (5) reduces to Eq. 6 for a specific temperature and dose rate. With a focus on the case of thermal degradation only, we set $\gamma = 0$ and the corresponding cumulative oxidation, $c(T, 0, t)$ in mol/g of the material after time t can be calculated using Eq. (7) given below. Further, an oxidation level given in mol/g is easily converted into % oxidation (mass % of reacted oxygen) using a multiplier of 32 g/mol times 100%.

$$r(T, \gamma, t) = \left(r(T_{ref}, 0, t_0) * \exp\left(\frac{E_1}{R} \left(\frac{1}{T_{ref}} - \frac{1}{T}\right)\right) + k\gamma^\alpha \exp\left(\frac{E_2}{R} \left(\frac{1}{T_{ref}} - \frac{1}{T}\right)\right) \right) * \left(\frac{t}{t_0}\right)^\alpha \quad (5)$$

$$r(T, \gamma, t) = r(T, \gamma, t_0) * \left(\frac{t}{t_0}\right)^\alpha \quad (6)$$

$$c(T, 0, t) = \frac{r(T, 0, t_0)}{t_0^\alpha (1 + \alpha)} (t^{1+\alpha} - t_0^{1+\alpha}) \quad (7)$$

5.2. Constant versus declining thermal oxidation/degradation rate

First, we focus on a time-independent case for thermal only conditions. The oxidation rate behavior for constant rates is shown in Fig. 20a, and the corresponding time-temperature superposition of the simulated cumulative percent oxidation is shown in Fig. 20b. For these simulations, we use the thermal only rates obtained from fitting the Eaton Dekoron Hypalon rate data using Model 4 which yielded a thermal E_a of 78.7 kJ/mol. The cumulative oxidation is linear with time, and thus exhibits a slope of 1 on the log-log plot shown in Fig. 20b. This is the expected behavior when time-dependence does not apply (i.e. constant rates).

We now compare this situation with a time-dependent case, where the oxidation rates decay with a power law defined by $\alpha = -0.1$. Fig. 21a shows the plots of simulated oxidation rates declining with time, again using interval times each of 72 h. Fig. 21b shows the time-temperature superposition of the resulting cumulative percent oxidation. The shift factors for this superposition yield an E_a of 87.4 kJ/mol. We recognize that the value of the thermal E_a is $1/0.9 = 11\%$ higher than the value obtained for the earlier example with constant rate. This demonstrates that the t-T superposition of rates that decline according to a power law with time will yield a higher ‘thermal E_a ’ than will an analysis that is based on constant rates.

Having different thermal E_a 's appears to contradict our model expectations with a single thermal E_a (Eq. (5)), however the two values (78.7 versus 87.4 kJ/mol) in this demo case are simply an example of the features of underlying time-dependence which we wished to illustrate. In particular, the E_a obtained from a time-temperature superposition of integrated oxidation with time dependence may not match a thermal E_a obtained from initial degradation rates.

5.3. Relationship between activation energies for thermal degradation

A relationship between the E_a 's for initial degradation rates and cumulative aging states is easily derived. We begin by establishing the temperature dependence of the oxidation rate and cumulative oxidation. If we define that the first oxidation rate measurement corresponds to an aging time t_1 , (assuming the same t_1 for all temperatures), we can apply Eq. (5) and Eq. (7) to this initial rate:

$$r(T, 0, t_1) = r(T_{ref}, 0, t_1) * \exp\left(\frac{E_a}{R} \left(\frac{1}{T_{ref}} - \frac{1}{T}\right)\right)$$

$$c(T, 0, t) = \frac{r(T_{ref}, 0, t_1)}{t_1^\alpha (1 + \alpha)} * \exp\left(\frac{E_a}{R} \left(\frac{1}{T_{ref}} - \frac{1}{T}\right)\right) * (t^{1+\alpha} - t_0^{1+\alpha})$$

$$\Rightarrow c(T, 0, t) \approx \frac{r(T_{ref}, 0, t_1)}{t_1^\alpha (1 + \alpha)} * \exp\left(\frac{E_a}{R} \left(\frac{1}{T_{ref}} - \frac{1}{T}\right)\right) * t^{1+\alpha}$$

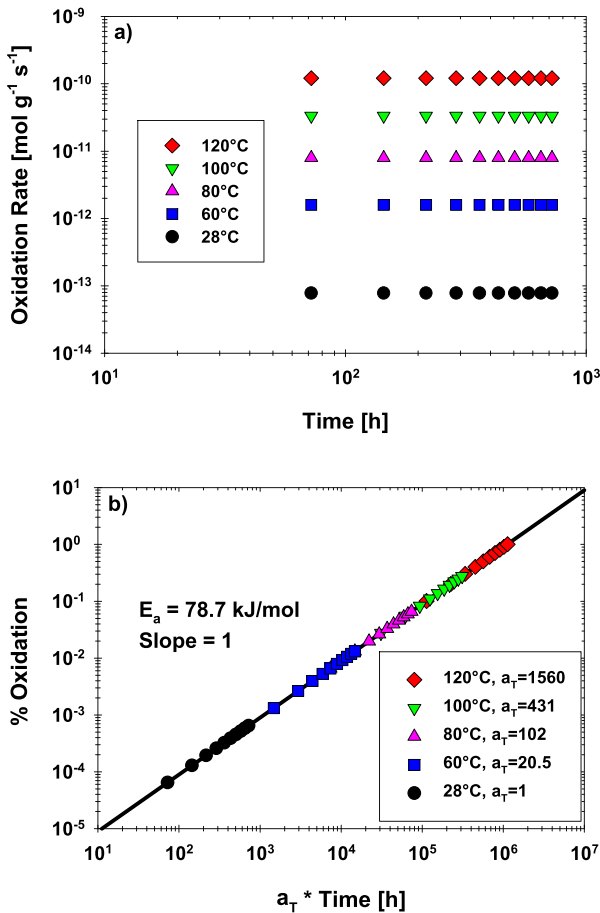


Fig. 20. (a) Simulated plots of oxidation rate versus cumulative aging time for constant oxidation rate. Oxidation rates are the projected thermal rates of the fit of Model 4 to the data for the Eaton Dekoron Hypalon jacketing material. (b) Oxidation levels (integrated oxidation rate) yield ideal time-temperature superposition with the E_a of 78.7 kJ/mol, the identical thermal E_a chosen for the simulation in a).

The next step is an approximation with the assumption that the time-temperature superposition is conducted for data at times that are much greater than t_0 . We can then see that a plot of $c(T, 0, t)$ against t on a log-log plot will be linear with slope $1+\alpha$ (the corresponding slope for the oxidation rate is α according to Eq. (5)). For the time-temperature superposition, the shift factor corresponding to temperature j may be expressed as $a_{Tj} = t_j/t_1$. To superpose all plots at elevated temperature to the plot at the reference temperature, we use these relationships.

$$\begin{aligned} c(T_{ref}, 0, a_{Tj} \cdot t_1) &= c(T_j, 0, t_1) \\ \Rightarrow \log(c(T_{ref}, 0, a_{Tj} \cdot t_1)) &= \log(c(T_j, 0, t_1)) \\ \Rightarrow (1 + \alpha) \cdot \log(a_{Tj} \cdot t_1) &= \frac{E_a}{R} \left(\frac{1}{T_{ref}} - \frac{1}{T_j} \right) + (1 + \alpha) \cdot \log(t_1) \\ \Rightarrow \log(a_{Tj}) &= \frac{E_a}{R(1 + \alpha)} \left(\frac{1}{T_{ref}} - \frac{1}{T_j} \right) \end{aligned} \quad (8)$$

Eq. (8) implies that an Arrhenius plot of the shift factors against inverse temperature will yield an E_a equal to the thermal rate E_a divided by the factor $1+\alpha$. For example, if the oxidation rate is

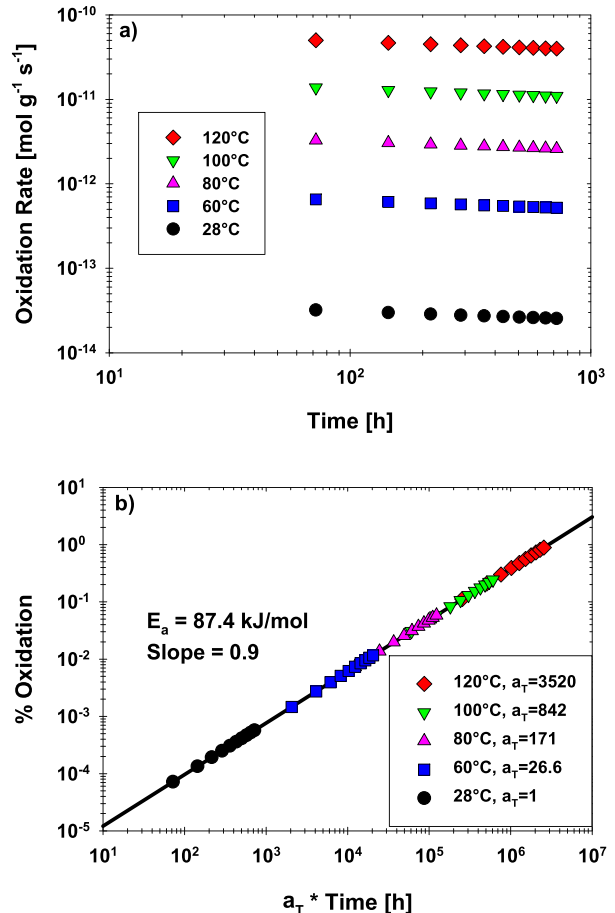


Fig. 21. (a) Simulated plots of oxidation rate versus cumulative aging time with a slowly declining oxidation rate according to a power law with time (Eaton Dekoron Hypalon initial rates from data fit with Model 4). The simulated oxidation rates decline with a slope of -0.1 . (b) The oxidation levels superpose onto a straight line using time-temperature superposition and yield a thermal E_a of 87.4 kJ/mol.

declining with slope on a log-log plot of $\alpha = -0.1$, then the slope of the % oxidation superposition will be 0.9. If we use an actual thermal rate $E_a = 78.7$ kJ/mol as before, the E_a obtained from superposition of such time-dependent data will thus be $78.7/(1-0.1) = 87.4$ kJ/mol, precisely the result shown in Fig. 21 (b). Consequently, when applying a time-temperature superposition to cumulative oxidation data that are influenced by rates that change over the experimental timeframe, the slope of the shift factors in an Arrhenius plot do not immediately represent the actual thermal rate E_a . Rather, it provides a value that depends on both the thermal rate E_a and the characteristic of the underlying time-dependence. Thus, to determine the thermal rate E_a for the initial material, one must consider how the oxidation rates change with time. The above example shows that if the time-dependent rates can be fitted to a power law model, the thermal rate E_a is especially easy to calculate.

Previous results for the near identical Samuel Moore Dekoron Hypalon material showed slowly decreasing oxidation rates over time (see Fig. IV-15 [5]) yielding a thermal E_a of 90.7 kJ/mol (see a_T values in Figure IV-17 [5]) from analysis of integrated oxidation levels over time. The slope of the t-T superposition in this plot is 0.87, which then gives an E_a for initial rates of 78.9 kJ/mol, which is in perfect agreement with our currently determined E_a of 79.4 kJ/mol for initial rates shown earlier in Fig. 19. Alternatively, with a decay of $\alpha = -0.13$ the measured E_a of 79.4 kJ/mol for initial rates converts to 91.3 kJ/mol for oxidation levels, consistent with 90.7 kJ/mol from the a_T values (37–108 °C in Figure IV-17 [5]) and

91 kJ/mol for two other Hypalon materials (shown in Fig. 27 of [16]).

5.4. General radiation-thermal model with a declining rate (example: power law)

This leads us to a general definition for a time-dependent radiation-thermal degradation model, shown below as Model 5. It is also possible to define expressions for **DED** and **TED** for particular functions defining time-dependency, for example a power law (Eq. (9) and Eq. (10)). Similarly, it would be possible to define separate time-dependency with distinctly different features for the thermal or radiative rate. Ultimately, feedback from measured rates and comparisons between models and actual aging data will help us refine time-dependent behavior. In fact, as will be shown later, constant oxidation rate behavior for combined environments offers good correlations between oxidation level and elongation at break suggesting that time dependence may likely not be a major concern for practical considerations. The derivations and plots below simply present an overview how significant time-dependence could appear in a **DED** plot.

rates, the curves superpose (low **DED** values) since in this region, the curves are linear on the log-log plot. We perform the superposition at a **DED** value of 10^4 Gy/h and the resulting shift factors are plotted in Fig. 23. Superposition yields an E_a of 90.5 kJ/mol, which is easily converted to 78.7 kJ/mol with a decay of -0.13 , which is precisely the thermal E_a for initial rates used in this example. **DED** plots in the linear thermal regime at low dose-rates will always have a slope of 1, with time-dependency given by the spacing along the x-axis as much as by the relative up and down position along the y-axis. A stronger decay in the degradation rate results in more pronounced spacing between different temperatures.

Since the exact time dependence of oxidation rates is not always available and impossible to predict, we are unfortunately faced with the situation that the interpretation of data from accelerated aging studies under radiation-thermal conditions will be subject to some uncertainty and likely divergence in quoted activation energies depending on the material property and data analysis method employed. Additional complexity may be introduced by synergistic coupling between the thermal and radiation processes that so far in the above mathematical derivations were not important.

$$r(T, \gamma, t) = (r_T + r_R)*f(t) = \left(r(T_{ref}, 0, t_0) * \exp\left(\frac{E_1}{R} \left(\frac{1}{T_{ref}} - \frac{1}{T}\right)\right) + k\gamma^\alpha \exp\left(\frac{E_2}{R} \left(\frac{1}{T_{ref}} - \frac{1}{T}\right)\right) \right) * f(t) \quad M5 - Eq. 1$$

Model 5: Example for a time-dependent model for degradation rate that combines Model 4 with a time-dependent function $f(t)$.

$$DED(\gamma, T) = \gamma \left[\frac{(1 + \alpha) * C * t_1^\alpha}{r(T, \gamma, t_1)} + t_0^{1+\alpha} \right]^{\frac{1}{1+\alpha}} \quad (9)$$

$$TED(\gamma, T) = \left[\frac{(1 + \alpha) * C * t_1^\alpha}{r(T, \gamma, t_1)} + t_0^{1+\alpha} \right]^{\frac{1}{1+\alpha}} \quad (10)$$

Using the fitted parameters of Model 4 to the rates for the Eaton Hypalon jacket material it is then possible to plot **DED** simulations, but now including time dependence for the combined degradation rate (using Eq. (9)). This plot is shown in Fig. 22 and was generated using $t_0 = 0.01$ h, $t_1 = 72$ h, and $\alpha = -0.13$. Again, we can apply horizontal dose rate superposition to these curves. At low dose

6. Performance predictions for combined radiation-thermal conditions based on oxidation rates

Performance predictions can be derived through modeling of **TED** (time to equivalent damage) with dose rate, where **TED** may represent dose, oxidation level, a specific reduced tensile elongation or any similar property. Predictions can be made in two ways by either using constant degradation rates as the fastest damage accumulation (but excluding any unexpected increase in rate), or by using a degradation rate that declines. For the latter approach, however, it may be difficult to verify that oxidation rates will continue to decline at all temperatures in a predictable manner and do not level off. Any predictions, whether rate based or using **DED**

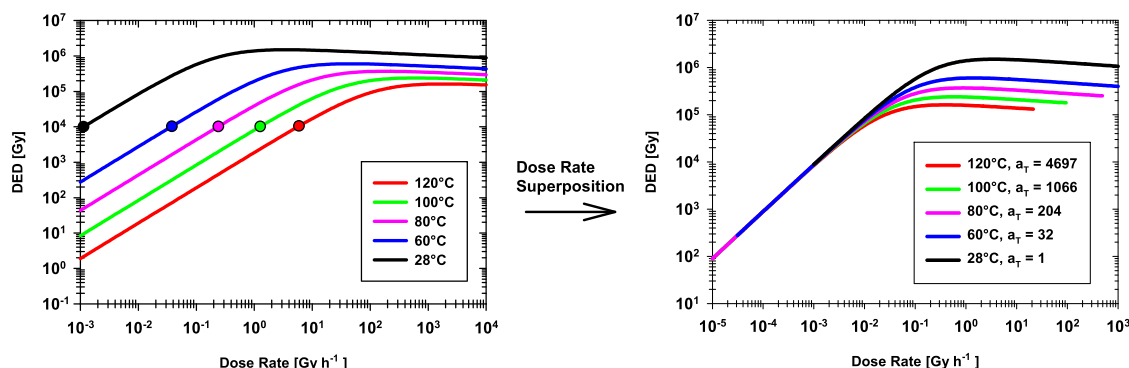


Fig. 22. Plot of simulated **DED** curves for Model 5 with embedded time dependence using the fitted parameters obtained from Model 4 (E_a of 78.7 kJ/mol) and a power law decay ($\alpha = -0.13$). These curves have a slope of 1 in the linear regime, but their spacing (in left plot) reflects the time dependence via the shift factors. They achieve their maximum values at intermediate dose rates as opposed to asymptotically approaching a maximum **DED** for each temperature at infinite dose rate (as was seen for models without considering time-dependent rates).

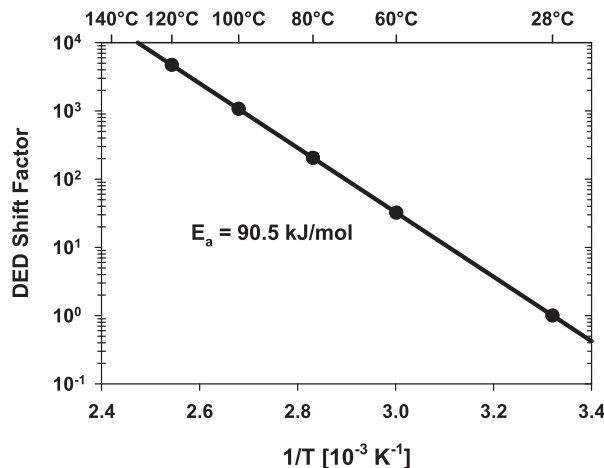


Fig. 23. Arrhenius plot of shift factors obtained by superposing curves in Fig. 22 at an isodose of 10⁴ Gy/h. Note that the extracted E_a from this plot matches the value obtained from the time-temperature superposition of oxidation levels for this material (see α_T values in Figure IV-17 [5]).

data with superposition and then assumptions for other combined environments [1,3,5,16,49] are subject to the same uncertainty, since we do not know how rates and material property changes will truly develop outside the existing data regime. Additional insight for changing chemistry was recently provided for the matched accelerated conditions (MAC) approach [16]. We also believe that a broad temperature - dose rate framework as shown throughout this study for the description of oxidation rates enables us to reduce uncertainty by better understanding overall material behavior. Prior to a computation with time dependence for the degradation rate, we show multiple scenarios for **TED** predictions involving oxidation with constant rate and its correlation with decreasing elongation at break (**EaB**).

Based on the time-independent Model 4 with the key assumption of constant degradation rates and two independent thermal and radiative pathways, predictions for the aging behavior of Eaton Dekoron Hypalon as a function of dose rate and temperature can be made using the expression for **TED** (Eq. (10) with $\alpha = 0$). For example, for environmental conditions of 0.6 Gy/h at 50 °C over 50 years (such an environment is consistent with extended nuclear power plant conditions at elevated temperature in some locations [6]), the measured oxidation rate data imply an accumulated oxidation level of ~4.9% based on a constant oxidation rate of 9.6*10⁻¹³ mol/g-s.

Some mechanical property data for aging of the Eaton Dekoron Hypalon at different combined environment conditions have not been published previously, but were retrieved for the current work. Fig. 24 shows the correlation between absolute **EaB** and oxidation levels calculated for the corresponding accumulated dose and time data using the rate parameters from Model 1 and Model 4 fitted to the newly measured oxidation rate data presented here for the first time. Fig. 24 shows evidence for divergence in the correlation between oxidation level and **EaB** for thermal dominated aging (0 and 56 Gy/h at 100 °C and higher temperatures) versus the other combined environments. Changes in the 'degradation chemistry mechanism' and hence different **EaB** for equal oxidation levels is a recognized complication for combined environment aging and the justification for the MAC approach to increase the predictive value of accelerated aging studies, but is much less common for thermal only aging (see later data for three elastomers). Interestingly, the oxidation rates obtained from Model 4 better emphasize the

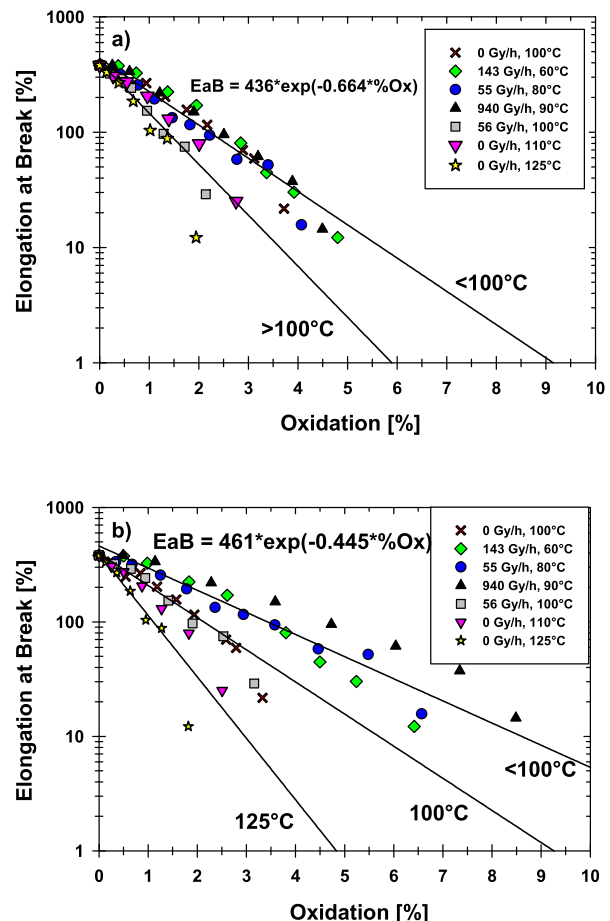


Fig. 24. Plot of elongation at break data for Eaton Dekoron Hypalon at a number of aging conditions (data previously unpublished) and plotted against calculated oxidation levels for the corresponding accumulated dose data using the fitted parameters for a) Model 1 and b) Model 4. Model 4 better emphasizes the drift in the correlation with increasing thermal dominated conditions.

increasing divergence between thermal dominated conditions and the radiative regime. Both models give validity to reasonably constant oxidation rates but also demonstrate differences in the dependence of elongation on oxidation level. Based on the existing aging data for the Eaton Dekoron CSPE and current rates an oxidation level of 6% suggests a significant reduction in mechanical properties with remaining elongation of ~25%.

Of fundamental interest is therefore a better understanding of the correlation between oxidation level and corresponding reduction in **EaB**. While not as good for the thermal dominated conditions, Fig. 24b demonstrates an underlying exponential relationship between oxidation level and elongation at break. A better illustration of the time-dependence of **EaB** and oxidation level is shown in Fig. 25 for 55 Gy/h at 80 °C, where the **EaB** shows a perfect exponential decay with time and oxidation level. Such correlations support our definitions of aging models based on oxidation rates and expectations for reasonably constant rates, with **EaB** then being a secondary property as a function of oxidation level. Perfect exponential decays are not expected for all materials and aging situations, but any other functional relationships could be easily established if more oxidation rate data were available for correlation with existing **EaB** aging data. In addition, there is also supporting evidence for reasonable exponential behavior in **EaB** and modulus for thermal aging of elastomers, for which constant

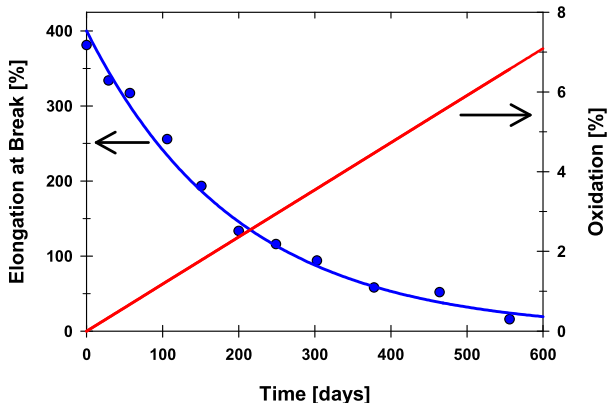


Fig. 25. Elongation at break and corresponding oxidation level presented in Fig. 24b for cumulative exposure at 80 °C and 55 Gy/h. For constant oxidation rate the oxidation level increases linearly with time, whereas the elongation at break exhibits perfect exponential decay.

oxidation rates have been verified. Fig. 26 shows an overview for three materials with **EaB** aging data superposed and referenced to cumulative oxidation using a constant oxidation rate at 80 °C for a chloroprene insulation material (2×10^{-11} mol/g-s [68]), a nitrile elastomer (4×10^{-11} mol/g-s [14,37]), and a PU binder material (4×10^{-11} mol/g-s [35]). For these materials 50% residual absolute **EaB** is reached after approximately 2.4% oxidation for the chloroprene, 3.7% for the nitrile, and 1.9% for the HTPB elastomer. Similarly, modulus changes (hardening) show near perfect exponential increases with respect to cumulative oxidation level for a number of materials [34–36]. Explanations for this apparently rather common exponential correlation between **EaB** and modulus with linear oxidation level in time are not readily available, but the once again observed exponential nature for the currently examined Eaton Dekoron Elastoset supports our notion for near constant oxidation rates as a foundation for Model 1 to 4.

Depending on a definition for remaining performance margin, e.g. 50 or 100% residual elongation or any similar property, and as long as a correlation with oxidation level is available, it is possible to express predicted ‘lifetimes’ as a function of dose rate and temperature. This concept is demonstrated in the Figures below (Fig. 27a–c), which shows the times required to reach iso-oxidation levels (1, 2, 5, 10% iso-damage states) or specific mechanical properties under any combined radiation-thermal conditions, derived as a boundary for constant oxidation rates with time (Model 4). Should the degradation process display subtle changes over time (for example some evidence for reduced oxidation rates as the degradation progresses) then the lifetime prediction will be more complicated and involve approximations based on the mathematics presented earlier. A similar situation will occur for higher temperatures when the additional thermal influence observed in Fig. 24b becomes important.

It is also possible to derive the corresponding DED plots for oxidation levels (M4-Eq. (2)), where Fig. 28a shows the doses required to reach different levels of oxidation at 50 °C, while Fig. 28b shows the temperature dependence of the dose to reach a 2% oxidation level. It is clear that superposition can only be accomplished in the temperature-dominated regime, as the low value for the radiative **Ea** in Model 4 contributes to the radiation-dominated DEDs. The **EaB** can be expressed as an exponential decay function of oxidation (%Ox) according to the equation below. Thus, the oxidation level as a function of **EaB** ($C(\epsilon)$) in [mol/g] can be used to calculate TED and DED values as before (e.g. the dose

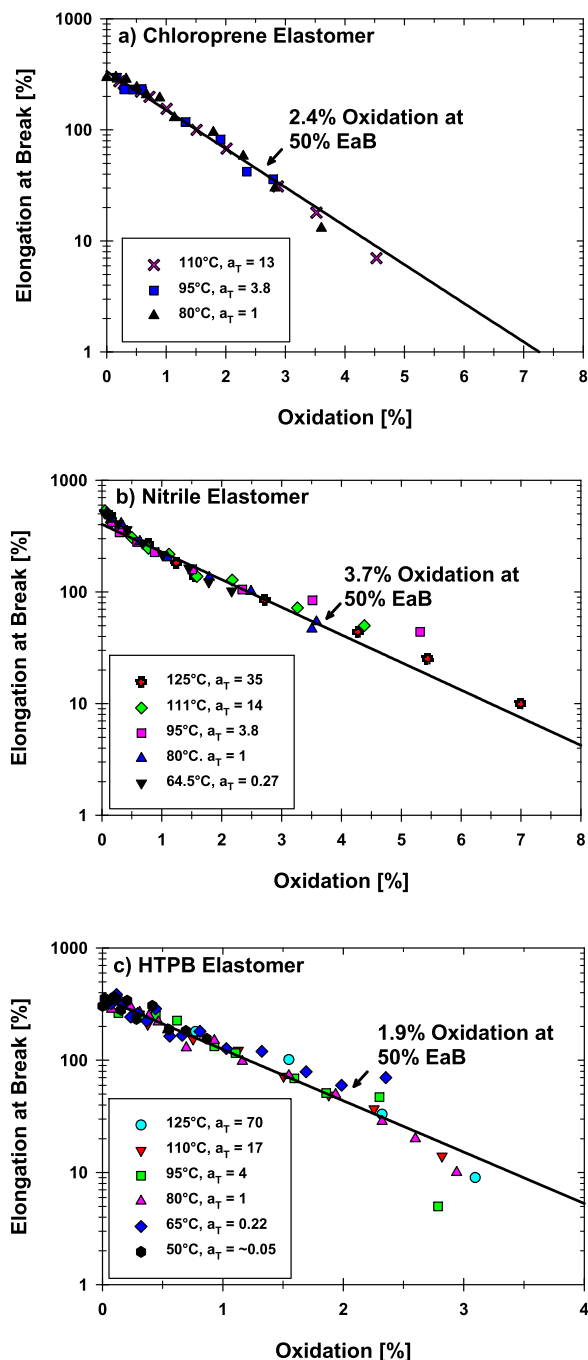


Fig. 26. Elongation at break and corresponding oxidation level for a) Rockbestos chloroprene [67], b) a nitrile rubber [37], and c) HTPB elastomer [35]. **EaB** data were initially time-temperature superposed and then referenced to cumulative oxidation at 80 °C.

required to reach 50% **EaB** is equal to the dose required to reach 1.6×10^{-3} mol/g, or 5% oxidation, see Fig. 24b for the Eaton Dekoron Hypalon fitted with Model 4). This is accomplished with the following relationship (with ϵ denoting elongation at break and ϵ_0 the **EaB** of the unaged material), where f_1 is an empirical factor ($f_1 = 0.445 \text{ } \%^{-1}$ for the Model 4 fit) and f_2 a conversion factor (3200 %·mol/g):

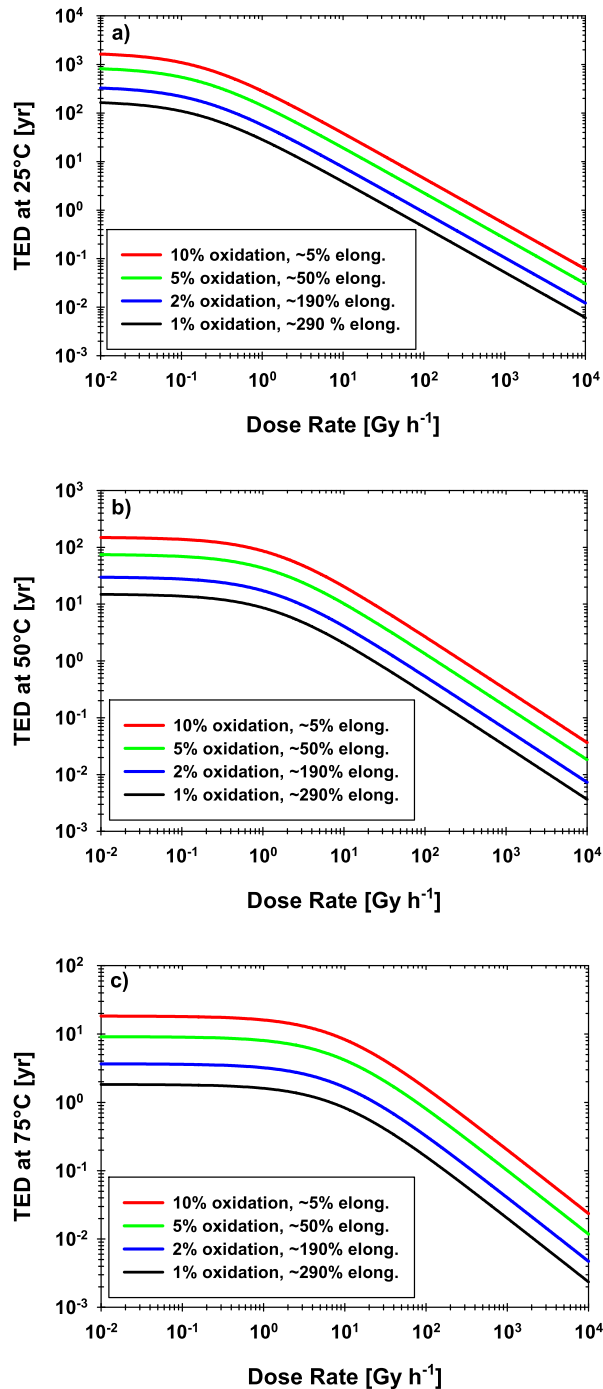


Fig. 27. Simulated curves of **TED** versus dose rate for four different oxidation levels (1, 5, 10%) using Model 4. Figs. a), b), and c) are simulated for different temperatures, here 25, 50, 75 °C, respectively. The plots show the expected aging times for the Eaton Dekoron Hypalon jacket material to reach between 1% and 10% oxidation and its corresponding predicted state for remaining tensile elongation at break.

$$\varepsilon = \varepsilon_0 e^{-f_1 * \% Ox} \quad C(\varepsilon) = \frac{\ln(\varepsilon_0 / \varepsilon)}{f_1 * f_2}$$

The resulting DED plots to reach different elongation values at 50 °C and 50% elongation at different temperatures are shown in Fig. 29a and b, respectively. In Fig. 29b the higher temperature (>100 °C) curves show reduced DED corresponding to the faster decay in elongation seen in Fig. 24b. The non-linear relationship

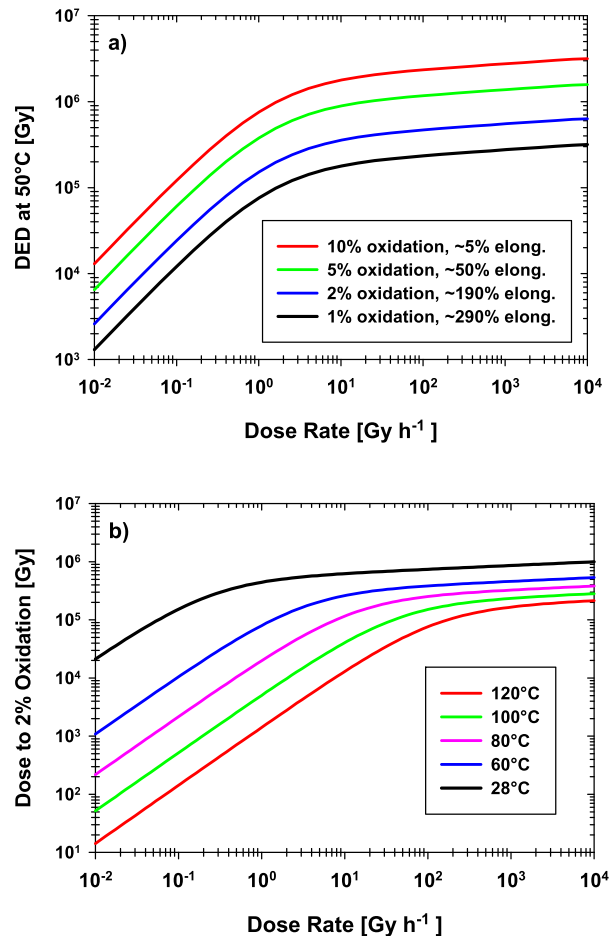


Fig. 28. Simulated **DED** curves versus dose rate for four different oxidation levels (1, 2, 5, 10%) using Model 4 at 50 °C (a) and DED to reach 2% oxidation at different temperatures (b).

between oxidation and elongation at break does not affect the shape of the DED curves, but rather the distance along the y-axis between different damage levels. Just like with the oxidation DED plots, temperature superposition can be achieved only in the thermal-dominated regions.

An example for performance predictions that incorporate time-dependency as defined by Model 5 is given below. Since the rates decline it will take longer to reach similar oxidation levels. This also changes the underlying correlation between elongation at break and its oxidation level. Fig. 30 shows an example for the Eaton Dekoron Hypalon with a rate decay of $\alpha = -0.13$. A similar loss in elongation as discussed above for 0.6 Gy/h at 50 °C will now require on the order of 100 years (see Fig. 31). Further, it is clear that the drawback for such predictions are assumptions for specific degradation rate behavior. In this case, the data for the highest dose rate diverge significantly, which is due to the limited influence of time-dependence during the much shorter aging exposure, and the temperature only data are compressed because the oxidation levels increase less when the rate decay is more important for longer aging times. The absence of an easily interpretable behavior suggests that time-dependence here likely does not apply as defined.

We recognize that once rates have been obtained oxidation progress can be easily modeled, but predictions for elongation at break are affected by additional thermal effects or changes in the correlation (Fig. 24b), which adds extra complexity for the high

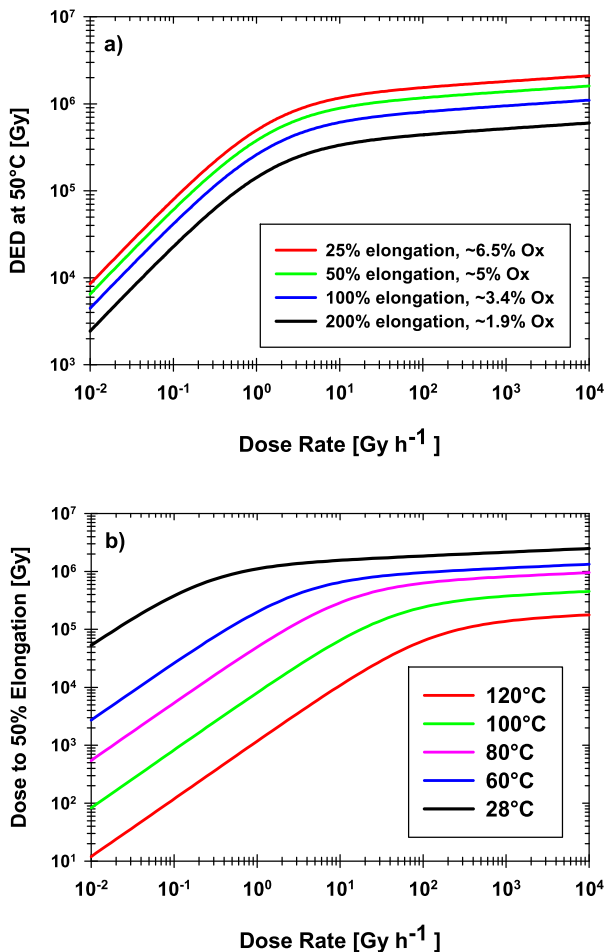


Fig. 29. Simulated curves of **DED** versus dose rate for four different levels of elongation at break (200, 100, 50, 25%) using Model 4 at 50 °C (a) and DED to reach 50% elongation at break at different temperatures (b), where the higher temperatures (>100 °C) display reduced DED corresponding to the faster decay in elongation seen in Fig. 24b.

temperature boundary for this material above 100 °C. While the trends in Fig. 24b may appear to discredit the use of this kinetic model and underlying assumptions, it is important to recognize that the thermal only behavior for the CSPE here is more complicated than expected, since other materials give excellent systematic correlations between **EaB** and oxidation level (Fig. 26). Further, it is clear that oxidation rates help us understand material behavior and can predict elongation nicely if the functional form and additional mechanistic changes are known. Our predictive capabilities could be improved by combining the MAC approach with oxidation rate measurements within the framework of these kinetic models. This is given by the fact that oxidation rates could be more easily experimentally obtained than changes in elongation when degradation proceeds slowly. Other jacketing and insulation materials may display more consistent correlations between elongation and oxidation level even under significantly different environments.

7. Approaches towards synergism between radiative and thermal pathways

A synergistic contribution provides an additional rate multiplier when radiation and temperature pathways interact in such a manner that oxidation/damage evolves faster than given by the

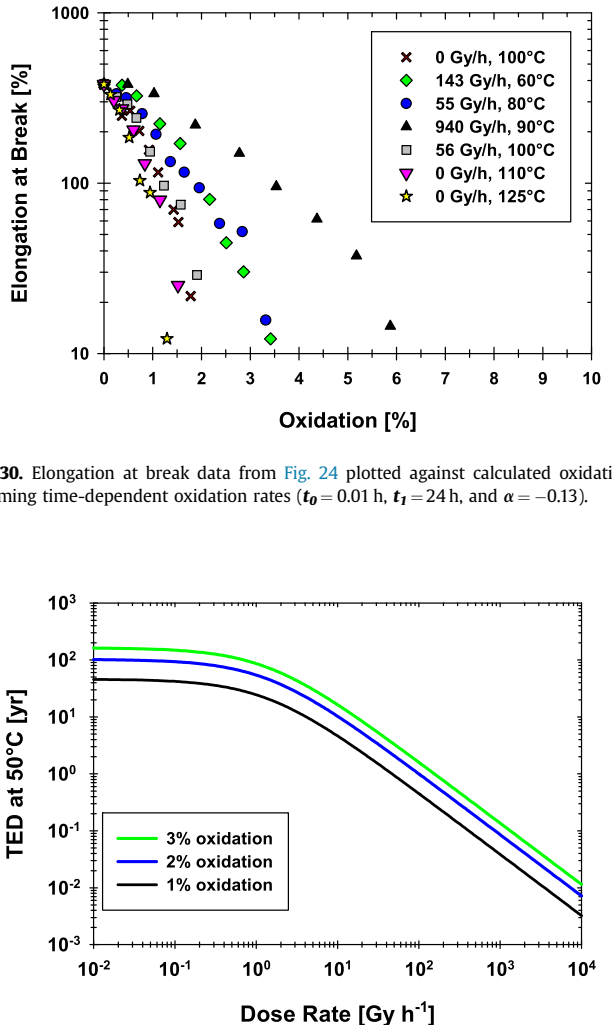


Fig. 30. Elongation at break data from Fig. 24 plotted against calculated oxidation assuming time-dependent oxidation rates ($t_0 = 0.01$ h, $t_1 = 24$ h, and $\alpha = -0.13$).

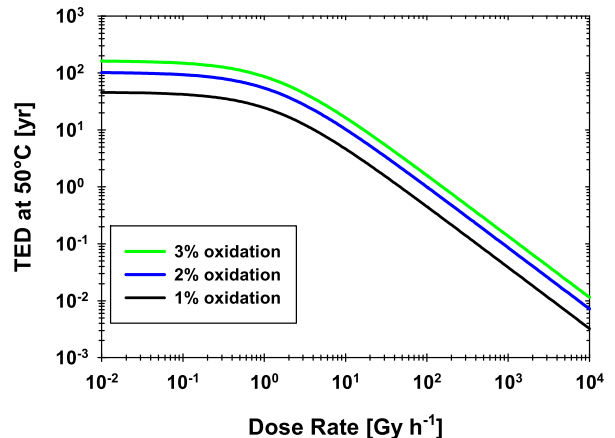


Fig. 31. Simulated TED curves to reach 1.2 and 3% oxidation at 50 °C using Model 5 with $t_0 = 0.01$ h, $t_1 = 24$ h, and $\alpha = -0.13$ for the Eaton Dekoron Hypalon jacket material.

simple sum of the two individual rates. Such synergism which results in an enhanced combined rate was recognized in the past by Ito [53,54], where the radiative rate was further associated with an additional **Ea** to explain the over-proportional increase in the combined rate.

$$r_{TR} > r_T + r_R \text{ and } r_R = c \gamma^\alpha e^{\left(\frac{-E_R}{kT}\right)} \quad [50-54].$$

In a similar manner, it is reasonable to define the combined rate as the sum of individual contributions including a rate for synergism **r_s**, (eq. (11)), which in itself can be defined as the sum of the thermal and radiative rates multiplied with **s**, a synergistic interaction parameter (eq. (12)). It is then possible to derive any synergistic contribution from experimental observations by comparing combined and individual rates (eq. (13)).

$$r_{TR} = r_S + r_T + r_R \quad (11)$$

$$r_S = s(r_T + r_R) \quad (12)$$

$$s = \frac{r_{TR} - (r_T + r_R)}{(r_T + r_R)} = \frac{r_{TR}}{(r_T + r_R)} - 1 \text{ or } r_{TR} = (1+s)(r_T + r_R) \quad (13)$$

This then leads to a few important recognitions. Firstly, there is no synergistic contribution if s equals zero, as r_s becomes zero and the combined rate simply matches the sum of the individual thermal and radiative rates. Secondly, if accelerated aging is considered such that r_T increases by a factor of x , and in parallel r_R increases by a factor of x , and this also results in the combined rate constant to increase by a factor of x , then s will remain constant for these specific temperature - dose rate conditions. Hence, there will be a synergistic multiplier, but its magnitude and functional relationship with temperature and dose rate is independent of similarly accelerated aging conditions. This also means ideal **DED** superposition will be maintained as long as this synergistic contribution occurs at the same relative rate conditions, i.e. the interactive parameter and functional form has its maximum contribution for example when $r_T = r_R$. In addition, in such equal acceleration situations, the effective synergism rate r_s will depend exactly on the thermal E_a or on the radiation dose rate.

We conclude that synergism can be present in combined aging environments, but absent any radiative E_a and if accelerated aging follows specific ideal behavior as defined above (matched accelerated conditions [16]), then the aging parameters (rates, DED, TED) will superpose and the synergistic interaction parameter will be constant. This represents an ideal condition for synergism, but has been observed based on the superposability of existing DED data sets, where however the magnitude of the synergistic contribution has not been determined [1,3,5,16]. It then becomes imperative, whenever 'increasing' or other synergism changes are discussed, to

on temperature. There is no expectation that the maximum value should increase with linear Arrhenius behavior, it could also be curved Arrhenius behavior with a changing E_a that increases with temperature, or any other suitable functional description.

- Experimental evidence is not yet available to confirm that a general synergism function describing the interaction parameter s displays the above attributes. However, absent any contradictory experimental evidence, these properties are a reasonable starting point. We also recognize that the $r_T = r_R$ condition for maximum contribution value defines a special, but not the broadest possible dose rate-dependent synergism function. For the most general case, a synergism function with a maximum contribution in the regions around this local thermal and radiation rate equivalency will need to be accommodated.
- Synergism may also show subtle time dependent behavior with changes in the synergism multiplier as the degradation and hence oxidation level progresses. Such a situation could be mathematically described.

Based on all earlier discussions, the most comprehensive radiation-thermal combined environment model that we can reasonably postulate is now given below as Model 6, which has significant degrees of freedom including an open function for time-dependency and general synergistic contribution. Both of these contributing functional multipliers can be specifically defined based on observed material behavior or preferred definitions such as an exponential decay in combined rates, exponent of 1 and zero E_a for the radiative rate, or constant maximum synergism interaction parameter.

$$\begin{aligned} r(T, \gamma, t) &= (r_T + r_R) * f(t) * f(T, \gamma) \\ &= \left(r(T_{ref}, 0, t_0) * \exp\left(\frac{E_1}{R}\left(\frac{1}{T_{ref}} - \frac{1}{T}\right)\right) + k\gamma^x \exp\left(\frac{E_2}{R}\left(\frac{1}{T_{ref}} - \frac{1}{T}\right)\right) \right) * f(t) * f(T, \gamma) \quad M6 - Eq. 1 \end{aligned}$$

Model 6: Most general model for degradation rate that combines Model 4 with a time-dependent function $f(t)$ and a function $f(T, \gamma)$ defining an interactive multiplier for synergism.

clearly distinguish between the synergistic interaction parameter (s , the added synergism multiplier) and the overall synergistic rate r_s that is governed by the thermal dependence of thermal and radiative rate. A more general and variable 'synergism' may exist in a number of ways, but some specific expected behaviors should offer a definition for the functional nature of the synergistic interaction parameter s :

- Synergism contributions will increase with dose rate and then decline, consistent with a transition from the thermal to the radiation dominated aging regimes where synergism must occur in-between.
- The synergistic interaction parameter is expected to be most effective when $r_T = r_R$, which then becomes the center of any multiplicative synergism function. At this condition the individual rates are not at their relative maximum, but at their strongest parallel condition.
- The synergism contribution could easily become more important with temperature as the thermal rate increases allowing for more interaction between the two pathways. Hence, its maximum value may require a unique dependence

As an overview of synergism when s increases with temperature and its influence on rate and **DED** or **TED** behavior for equal oxidation levels, we focus on the most basic Model 1 ($x = 1$ and $E_2 = 0$, and for now no time-dependence in Model 6) and define a Gaussian distribution function that yields s and increases in its maximum value with temperature at $r_T = r_R$ (for simple demonstration purposes here having a relative maximum of 0.25 at 28 °C and 1 at 120 °C) using a constant E_a of 15 kJ/mol. Further, we define the width of the Gaussian synergistic parameter function by reaching 25% of its intensity within a decade of lower or higher dose rate. The low and high dose rate boundaries for this function are 0. The shape of the log-normal distribution, $f(T, \gamma)$, in terms of its mean (μ) and standard deviation (σ , set to 1.39 to obtain a suitable peak width) is defined in Eq. (14), where one is added to yield an overall synergistic rate multiplier for the sum of $r_T + r_R$; f_{ref} is the maximum at the reference temperature, and E_3 is the activation energy of the peak height. Further, the temperature dependence of the mean is given in Eq. (15) and the dose-rate at which $r_T = r_R$ ($\gamma_{rT=rR}$) is defined according to Eq. (16). The resulting synergistic multiplier functions are shown in Fig. 32 with increasing temperature.

$$f(T, \gamma) = 1 + \frac{\gamma_{rT=rR} * \exp\left(\frac{(\ln(\gamma_{rT=rR}) - \mu(T))^2}{2\sigma^2}\right) * f_{ref} * \exp\left(\frac{E_a}{R} \left(\frac{1}{T_{ref}} - \frac{1}{T}\right)\right)}{\gamma} = 1 + s \quad (14)$$

$$\mu(T) = \sigma^2 + \ln(\gamma_{rT=rR}(T)) \quad (15)$$

$$\gamma_{rT=rR}(T) = \frac{r(T_{ref}, 0) * \exp\left(\frac{E_a}{R} \left(\frac{1}{T_{ref}} - \frac{1}{T}\right)\right)}{k} \quad (16)$$

We select simple parameters for the overview Model 1, i.e. 80 kJ/mol for a thermal rate and the related values used in Fig. 2 to obtain the relevant plots for rate and **DED** behavior. The solid lines in Fig. 33 show the synergistic contributions as deviations from the curves according to Model 1 which excludes added synergism (hyphenated). As intended the synergistic contribution adds to the degradation rate around the $r_T = r_R$ condition. The synergism contribution is best demonstrated by comparing two specific **DED** curves for 2% oxidation as shown in Fig. 34. Synergism is of little importance at the lowest temperature, but results in faster degradation at 100 °C for the higher dose rates in comparison with the expected behavior from Model 1.

When the synergism factor increases with temperature (due to E_3 in Eq. (14)), it is clear that rate and **DED/TED** data are then no longer fully superposable. As mentioned earlier, ideal **DED** superposition will only be maintained when a specific synergism function is independent of temperature and dose rate (i.e. $E_3 = 0$ in Eq. (14)), and has identical shape and constant maximum value at the $r_T = r_R$ condition. Such constraints are unlikely for all aging situations, but have been suggested by Gillen as arguments for non-changing ‘interactive’ parameters when fully superposable aging data exist, yet synergism also applies [1,3,16]. Therefore, perfect superposition of **DED** data for multiple temperatures is no longer expected when more complex synergism contributes to the aging behavior. Any synergism is easily visualized as deviations from ideal behavior in rate or **DED** plots, even for the most basic Model 1 discussed in this overview (for example in Figs. 33 and 34).

Another important observation in Fig. 33 is the significantly

enhanced degradation rate predicted for higher dose rates above 80 °C when the growing synergism applies as shown in Fig. 32. This is factually consistent with our rate measurements shown in Fig. 11, which earlier resulted in a requirement of adding a secondary radiative E_a to the aging model. This now leads to an intriguing conclusion, namely that a growing synergistic contribution is consistent with a secondary radiative E_a , at least in the dose rate regime that has been experimentally accessible here. Hence, the observations of a secondary E_a for the radiative term by Burnay [49] and Ito [51–53] are also consistent with growing importance of synergism through increases in the synergistic interaction parameter. Whether this contribution decays towards much higher dose rates, as would be expected for a centered synergism function, or is maintained as given by all other models with an independent radiative E_a remains to be established. In terms of predictive accelerated aging studies, much higher dose rate experiments are certainly less attractive due to DLO and reduced influence of thermal contributions.

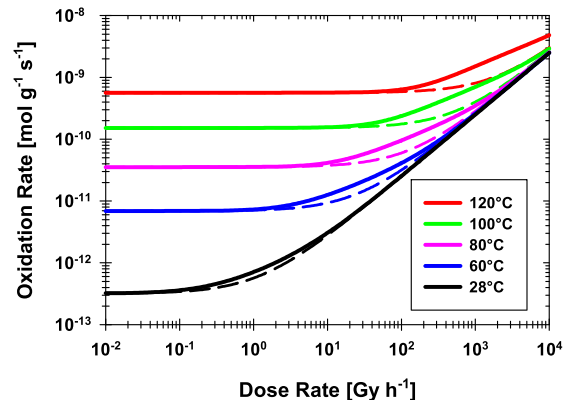


Fig. 33. Simulated synergism functions added to the rate plots for Model 1 and the overview given in Fig. 2. Dashed lines represent the rates without synergism, and solid lines include the synergistic interaction parameter multiplier.

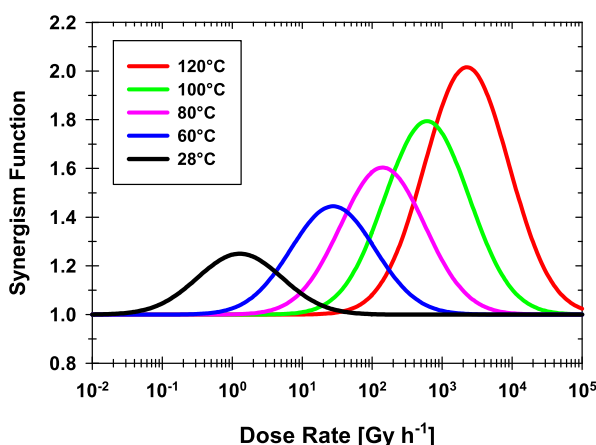


Fig. 32. Simulated synergism functions using a Gaussian definition with a maximum value at $r_T = r_R$ for the overview behavior (Model 1) shown in Fig. 2 and increasing intensity with an E_a of 15 kJ/mol.

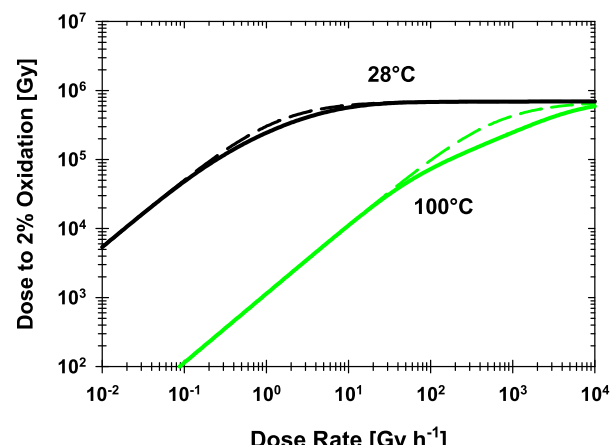


Fig. 34. Effect of synergism (solid lines) on the **DED** data for two temperatures in Fig. 2 (Model 1). At the higher temperature the deviation between ideal and accelerated degradation due to growing synergism becomes more important.

8. Conclusions

An overview of the interpretation of accelerated aging behavior under combined radiation-thermal oxidative environments has been presented. Being more complicated than traditional thermal aging, experimental planning and data interpretation need to include thermal as well as radiative degradation pathways that have been regarded as the sum of independent parallel processes without additional synergism in the past (see existing literature [1,3,7,14,16]). No aging model so far has offered a rigorous mathematical definition of synergistic behavior leading to an amplification of the combined effect of concurrent thermal and radiation driven processes. Furthermore, no previous aging models have incorporated synergism into a systematic description with definitions for oxidatively driven degradation rate, **DED**, **TED** and underlying shift factors (see overview equations for aging Models 1 to 4 in this work). An introductory model for synergism has therefore been proposed in this overview. Further, for appropriate data interpretation, we also require the absence of any DLO contributions under accelerated aging conditions, meaning that material oxidation and associated changes in mechanical properties are expected to proceed homogenously [1,4,13,45]. For the work here we also discount any ‘inverse temperature’ phenomena [32,33].

8.1. Avenues for expanded combined environment aging models

We wish to emphasize that the original degradation model (Gillen and Clough in 1989 [1], and its foundation for Burnay's model in 1990 [49]) has provided excellent fits to many data sets for the interpretation of combined radiation-thermal environments (see existing literature [1,3,5,16]). Only small deviations from ‘ideal aging behavior’ need to be better accommodated ([49]), which then becomes a question of perhaps accepting extra complexity in the radiation regime, any contributions from synergism, or additional time-dependence in oxidation rates. Moving beyond the existing basic model and in agreement with its modified version (Burnay and Rudd in 1990 [49]), further evidence is provided that an additional E_a for the radiative contribution to the oxidation rate under high dose rate conditions may offer improved fits, as was shown here for a chlorosulfonated polyethylene (Hypalon) cable jacket material. Existing data for many materials may be fitted sufficiently well without the high dose rate regime needing an additional E_a . This is perfectly acceptable, because a global model fit will establish the best parameters, and the secondary E_a could trend towards zero. We also wish to point out that not all materials may require an additional E_a term for radiation. Rather, we offer strategies for a broader radiation-thermal kinetic model to include an extra degree of freedom, such as an additional radiative E_a or a synergistic pathway, that may better fit some data sets that show non-ideal behavior at high dose-rate and temperature conditions. Our improved model descriptions introduced here (Model 4 to 6) offer alternative options to combine thermal and radiative activation energies into a general kinetic model for a convoluted aging process including synergism and non-constant degradation rates. However, within the limits of available experimental data, any clear distinctions between these multiple degrees of freedom may not be possible. As we have demonstrated, we are reaching the point where data sets can be equally well described with different models and subjective interpretation.

8.2. Determination of activation energies and validation of aging model

DED - dose rate superposition analysis is the established method in the literature for the evaluation of combined environment aging

data and the determination of a thermal E_a . However, by default the **DED** approach requires superposability to be valid based on the definition of the aging model. As we have shown, subtle modifications to an aging model may no longer enable perfect superposability, yet still offer excellent data fits and thereby yield the underlying thermal E_a . We introduced and wish to emphasize the attractiveness to easily fit complete data sets to a global kinetic model using residual error minimization methods. Any well-defined aging model can be easily evaluated by individually or simultaneously fitting oxidation rate, **DED** or **TED** data to clarify the underlying thermal and any radiative dependencies in the given temperature - dose rate regime. Further, an additional advantage of the global model fitting approach is given by the fact that non-linearity, i.e. deviations from ‘ideal’ behavior, can be easily evaluated by comparing predicted/simulated trends versus actual data. As was shown for some cases, a global curve fit of all data points will be the only approach to accurately describe the underlying material degradation behavior, for example when **DED** superposition cannot be conducted at all damage levels due to imperfect superposition behavior (i.e. high dose rate behavior for Model 4).

8.3. Determination of E_a at fixed dose rate has no predictive value

We emphasized through rigorous analysis that under combined thermal radiation conditions, it is not possible to select a fixed dose rate and conduct ‘meaningful’ thermal aging equivalent experiments for different temperatures. An expectation for a representative E_a from such experiments is simply incorrect and will not have predictive value outside of the narrow scope of the aging conditions unique to the experiment. Firstly, such data sets can only yield linear Arrhenius behavior in the thermal dominated region, and secondly an ‘average E_a ’ which will be obtained within the boundaries of pure thermal conditions (low dose rate) and the radiation dominated regime (high dose rates) would incorrectly suggest lower rates at lower temperatures. Degradation rates can only be predicted through knowledge of the thermal E_a and an applicable aging model for combined environment conditions. Alternative approaches for predictions may be found in the matched accelerated conditions (MAC approach) [16].

8.4. Complications when oxidation rates show subtle time behavior

Any underlying time dependence in oxidation rates, for example a decrease as oxidation and aging levels evolve, means that different thermal E_a 's will be obtained if initial oxidation rates or **DED** data (equally cumulative oxidation or % elongation at break vs. time) are used for its determination. While we do not yet have a complete understanding of the underlying physical basis of time-dependent rate behavior, it has been observed in several different materials and can have significant impact on lifetime predictions that are based on correlations between mechanical property changes and cumulative oxidation levels based on initial rates. Knowing time-dependency of the degradation rate allows us to compare the relevant E_a 's. Again, for some degradation models, the thermal E_a cannot be elucidated by data superposition alone. Rather, a global model fit to the experimental data is the only method to yield the embedded E_a 's.

8.5. Better performance predictions based on oxidation behavior

The goal of all accelerated aging studies is performance predictions for lower dose rate and lower temperature conditions. Oxidation rate data taken in the early stages of degradation offer additional guidance for aging conditions that have little immediate impact on mechanical properties. This enables data input into

global models that cover a larger aging regime than usually accessible with **DED** data. **DED** superposition analysis [1,3] including more meaningful aging conditions [16], describes data often very well and can be predictive, but has more uncertainty in the low dose rate thermal regime subject to unknown rate behavior. Further, oxidation levels can be correlated with elongation data, and rate-based models can then enable **TED** (time to equivalent damage) projections for specific aging states to be derived, either under constant or declining rate conditions. With constant oxidation rates, multiple materials showed excellent exponential decays for elongation at break data, which would be first order behavior if it could be associated with definable degradation chemistry. Rate based global models allow us to explore boundary conditions for material behavior as well as predictions for specific circumstances. However, we also recognize that any predictions that move from accelerated conditions towards lower temperatures and dose rates remain subject to uncertainty in the exact rate behavior. Outstanding issues include mechanistic changes with dose rate that affect the correlation between oxidation level and elongation at break. Such trends have recently been addressed with more targeted matched accelerated conditions [16].

8.6. Synergism between radiation and thermal pathways

Another area that has lacked clarifications in the past are deviations from basic aging models due to additional synergism between the thermal and radiation driven degradation pathways. An approach towards synergism was developed via the definition of a Gaussian rate multiplier function that increases in importance with temperature at the mid-point between the radiation and thermal dominated regime. A growing synergistic interaction parameter is consistent with an additional E_a for the radiative component. However, with the addition of a radiative E_a or temperature-dependent synergistic multipliers, ideal **DED** superposition is no longer possible. Supporting experimental evidence for synergism has been recently provided in an independent parallel publication [71].

8.7. Current status and forward looking directions

In summary, this overview offers an in-depth perspective on different approaches for the interpretation of oxidation rates and aging data evolution with temperature and dose rate. Importantly, we recognize that a basic kinetic model allowing for superposition of **DED** data already describes many aging data sets very well. For enhanced fits an improved kinetic aging model was introduced (Model 4) and applied to a comprehensive set of experimental oxidation rates. Any aging predictions (see **TED** plots in section 6) will have uncertainty without a systematic understanding of material behavior over a large dose rate - temperature regime and an aging model with sufficient degrees of freedom to accommodate non-ideal behavior. Aging models can be further expanded through the incorporation of time-dependence for rates, the addition of a radiative E_a term, and additional synergism functions resulting in the definition of the most comprehensive Model 6.

While we focused on the description of oxidation rates, their time-dependence and correlation with elongation, and introduced the concept of synergism for higher dose rate and temperature conditions, these aging models should be equally applicable to **DED** data involving elongation. The recent concept for matched accelerated conditions (MAC approach) as more meaningful aging conditions to avoid changes in correlations between aging chemistry and mechanical property changes [16], would need to be discussed within the boundaries of a single thermal E_a (as used in [16]) or with the consequences of an additional radiative E_a , which may be equally given by an increasing synergistic interaction parameter.

The existing **DED** and MAC approaches have a limited mathematical framework for underlying oxidation behavior. Our predictive capabilities could be improved by combining the MAC approach with oxidation rate measurements within the framework of these kinetic models. This is given by the fact that oxidation rates could be more easily experimentally obtained than changes in elongation when degradation proceeds slowly. Additionally, it may be impossible to successfully deconvolute aging data in terms of synergism contributions versus the presence of an underlying radiative E_a or potential time-dependent rate behavior. Looking forward, any preference for another modified model and data analysis requires absolute clarity for the functional definitions of the oxidation/degradation rate, **DED/TED**, E_a 's and a_T with temperature and dose rate. This then allows global fits with different models to be more easily compared and any differences to be highlighted. For meaningful progress in this field, ideally any preferred model should be compared with others to justify why a particular solution is best.

Acknowledgements

Sandia National Laboratories is a multi-mission laboratory managed and operated by National Technology and Engineering Solutions of Sandia, LLC, a wholly owned subsidiary of Honeywell International, Inc., for the U.S. Department of Energy's National Nuclear Security Administration under contract DE-NA0003525. We gratefully acknowledge ongoing technical support at the LICA facility and the repeated sample handling provided by Don Hanson and Maryla Wasiolek for oxidation rate measurements. We also recognize and thank Ken Gillen for many useful comments and critical opinions. Note: This paper describes objective technical results and analyses. Any subjective views or opinions that might be expressed in the paper do not necessarily represent the views of the U.S. Department of Energy or the United States Government.

References

- [1] K.T. Gillen, R.L. Clough, Time-temperature-dose rate superposition: a methodology for extrapolating accelerated radiation aging data to low dose rate conditions, *Polym. Degrad. Stabil.* 24 (1989) 137.
- [2] K.T. Gillen, R.L. Clough, Quantitative confirmation of simple theoretical models for diffusion-limited oxidation, in: R.L. Clough, S.W. Shalaby (Eds.), *Radiation Effects on Polymers*, ACS Series #475, ACS, Washington, D.C., 1991, p. 457.
- [3] K.T. Gillen, R.L. Clough, Predictive aging results in radiation environments, *Radiat. Phys. Chem.* 41 (1993) 803.
- [4] J. Wise, K.T. Gillen, R.L. Clough, Time development of diffusion-limited oxidation profiles in a radiation environment, *Radiat. Phys. Chem.* 49 (1997) 565.
- [5] K.T. Gillen, R.A. Assink, R. Bernstein, *Nuclear Energy Plant Optimization (NEPO): Final Report on Aging and Condition Monitoring of Low-Voltage Cable Materials*, Sandia National Laboratories, Albuquerque and Livermore, 2005, pp. SAND2005–7331.
- [6] M.C. Celina, K.T. Gillen, E.R. Lindgren, *Nuclear Power Plant Cable Materials: Review of Qualification and Currently Available Aging Data for Margin Assessments in Cable Performance*, Sandia National Laboratories, 2013. SAND 2013-2388.
- [7] M. Celina, E. Redline, R. Bernstein, N. Giron, A. Quintana, G. White II, *Summary Report of Cable Aging and Performance Data for Fiscal Year 2014*, Sandia National Laboratories, 2014. SAND 2014-17779.
- [8] K.T. Gillen, R.L. Clough, A kinetic model for predicting oxidative degradation rates in combined radiation-thermal environments, *J. Polym. Sci. Polym. Chem. Ed.* 23 (1985) 2683.
- [9] T. Yamamoto, T. Minakawa, *The Final Report of the Project of "Assessment of Cable Aging for Nuclear Power Plants*, Japan Nuclear Energy Safety Organization (JNES), Tokyo, 2009. JNES-SS-0903.
- [10] Expanded Materials Degradation Assessment (EMDA) Volume 5: Aging of Cables and Cable Systems, 2014. NUREG/CR-7153, Vol. vol. 5.
- [11] T. Seguchi, K. Tamura, T. Ohshima, A. Shimada, H. Kudoh, Degradation mechanisms of cable insulation materials during radiation-thermal ageing in radiation environment, *Radiat. Phys. Chem.* 80 (2010) 268.
- [12] T. Seguchi, K. Tamura, A. Shimada, M. Sugimoto, H. Kudoh, Mechanism of antioxidant interaction on polymer oxidation by thermal and radiation ageing, *Radiat. Phys. Chem.* 81 (2012) 1747.

- [13] M.C. Celina, Review of polymer oxidation and its relationship with materials performance and lifetime prediction, *Polym. Degrad. Stabil.* 98 (2013) 2419.
- [14] K.T. Gillen, R. Bernstein, M. Celina, Challenges of accelerated aging techniques for elastomer lifetime predictions, *Rubber Chem. Technol.* 88 (2015) 1.
- [15] J. Verdu, *Oxidative Ageing of Polymers*, ISTE Ltd and John Wiley & Sons Inc, Hoboken, 2012.
- [16] K.T. Gillen, M. Celina, Predicting polymer degradation and mechanical property changes for combined radiation-thermal aging environments, *Rubber Chem. Technol.* 91 (2018) 27.
- [17] K.T. Gillen, M. Celina, M.R. Keenan, Methods for predicting more confident lifetimes of seals in air environments, *Rubber Chem. Technol.* 73 (2000) 265.
- [18] K.T. Gillen, R. Bernstein, Review of Nuclear Power Plant Safety Cable Aging Studies with Recommendations for Improved Approaches and for Future Work, Sandia National Laboratories, Albuquerque and Livermore, 2010. SAND 2010-7266.
- [19] L. Audouin, X. Colin, B. Fayolle, E. Richaud, J. Verdu, *Polymeres en ambience nucleaire*, EDP Sciences, 2012.
- [20] M. Sugimoto, A. Shimada, H. Kudoh, K. Tamura, T. Seguchi, Product analysis for polyethylene degradation by radiation and thermal ageing, *Radiat. Phys. Chem.* 82 (2013) 69.
- [21] A. Shimada, M. Sugimoto, H. Kudoh, K. Tamura, T. Seguchi, Radiation ageing technique for cable life evaluation of nuclear power plant, *IEEE Trans. Dielectr. Electr. Insul.* 19 (2012) 1768.
- [22] A. Shimada, M. Sugimoto, H. Kudoh, K. Tamura, T. Seguchi, Degradation distribution in insulation materials of cables by accelerated thermal and radiation ageing, *IEEE Trans. Dielectr. Electr. Insul.* 20 (2013) 2107.
- [23] A. Shimada, M. Sugimoto, H. Kudoh, K. Tamura, T. Seguchi, Degradation mechanisms of silicone rubber (SiR) by accelerated ageing for cables of nuclear power plant, *IEEE Trans. Dielectr. Electr. Insul.* 21 (2014) 16.
- [24] T. Seguchi, K. Tamura, H. Kudoh, A. Shimada, M. Sugimoto, Degradation of cable insulation material by accelerated thermal radiation combined ageing, *IEEE Trans. Dielectr. Electr. Insul.* 22 (2015) 3197.
- [25] Assessment and Management of Ageing of Major Nuclear Power Plant Components Important to Safety: In-Containment Instrumentation and Control Cables, International Atomic Energy Agency, Vienna, 2000. IAEA-TECDOC-1188.
- [26] A. Chapiro, *Radiation Chemistry of Polymeric Systems*, Interscience Publishers, 1962.
- [27] F.A. Makhlis, *Radiation Physics and Chemistry of Polymers*, Keter Publishing House Jerusalem Ltd., 1975.
- [28] R.J. Woods, A.K. Pikaev, *Applied Radiation Chemistry Radiation Processing*, John Wiley & Sons, Canada, 1994.
- [29] M. Dole (Ed.), *The Radiation Chemistry of Macromolecules I*, Academic Press, 1972.
- [30] M. Dole (Ed.), *The Radiation Chemistry of Macromolecules II*, Academic Press, 1973.
- [31] M. Celina, G.A. George, Characterization and degradation studies of peroxide and silane crosslinked polyethylene, *Polym. Degrad. Stabil.* 48 (1995) 297.
- [32] M. Celina, K.T. Gillen, J. Wise, R.L. Clough, Anomalous aging phenomena in a crosslinked polyolefin cable insulation, *Radiat. Phys. Chem.* 48 (1996) 613.
- [33] M. Celina, K.T. Gillen, R.L. Clough, Inverse temperature and annealing phenomena during degradation of crosslinked polyolefins, *Polym. Degrad. Stabil.* 61 (1998) 231.
- [34] M. Celina, J. Wise, D.K. Ottesen, K.T. Gillen, R.L. Clough, Oxidation profiles of thermally aged nitrile rubber, *Polym. Degrad. Stabil.* 60 (1998) 493.
- [35] M. Celina, A.C. Graham, K.T. Gillen, R.A. Assink, L.M. Minier, Thermal degradation studies of a polyurethane propellant binder, *Rubber Chem. Technol.* 73 (2000) 678.
- [36] M. Celina, J. Wise, D.K. Ottesen, K.T. Gillen, R.L. Clough, Correlation of chemical and mechanical property changes during oxidative degradation of neoprene, *Polym. Degrad. Stabil.* 68 (2000) 171.
- [37] J. Wise, K.T. Gillen, R.L. Clough, An ultrasensitive technique for testing the Arrhenius extrapolation assumption for thermally aged elastomers, *Polym. Degrad. Stabil.* 49 (1995) 403.
- [38] J. Wise, K.T. Gillen, R.L. Clough, Quantitative model for the time development of diffusion-limited oxidation profiles, *Polymer* 38 (1997) 1929.
- [39] K.T. Gillen, M. Celina, The wear-out approach for predicting the remaining lifetime of materials, *Polym. Degrad. Stabil.* 71 (2000) 15.
- [40] K.T. Gillen, E.R. Terrill, R.M. Winter, Modulus mapping of rubbers using micro- and nano-indentation techniques, *Rubber Chem. Technol.* 74 (2001) 428.
- [41] K.T. Gillen, R.A. Assink, R. Bernstein, Condition monitoring approaches applied to a polychloroprene cable jacketing material, *Polym. Degrad. Stabil.* 84 (2004) 419.
- [42] J.E. Pickett, D.A. Gibson, S.T. Rice, M.M. Gardner, Effects of temperature on the weathering of engineering thermoplastics, *Polym. Degrad. Stabil.* 93 (2008) 684.
- [43] J.E. Pickett, D.A. Gibson, M.M. Gardner, Effects of irradiation conditions on the weathering of engineering thermoplastics, *Polym. Degrad. Stabil.* 93 (2008) 1597.
- [44] O. Haillant, Accelerated weathering testing principles to estimate the service life of organic PV modules, *Sol. Energy Mater. Sol. Cells* 95 (2011) 1284.
- [45] A. Quintana, M.C. Celina, Overview of DLO modeling and approaches to predict heterogeneous oxidative polymer degradation, *Polym. Degrad. Stabil.* 149 (2018) 173.
- [46] E. Linde, N.H. Giron, M.C. Celina, Water diffusion with temperature enabling predictions for sorption and transport behavior in thermoset materials, *Polymer* 153 (2018) 653.
- [47] R.L. Clough, K.T. Gillen, Combined environment aging effects: radiation-thermal degradation of poly(vinyl chloride) and polyethylene, *J. Polym. Sci. Polym. Chem. Ed.* 19 (1981) 2041.
- [48] R.L. Clough, K.T. Gillen, Investigation of cable deterioration inside reactor containment, *Nucl. Technol.* 59 (1982) 344.
- [49] S.G. Burnay, A practical model for prediction of the lifetime of elastomeric seals in nuclear environments, in: R.L. Clough, S.W. Shalaby (Eds.), *Radiation Effects on Polymers*, ACS Series #475, ACS, 1991, p. 524.
- [50] M. Ito, Chemorheology of rubber under heat and radiation, *Radiat. Phys. Chem.* 18 (1981) 653.
- [51] M. Ito, Application of chemorheology to radiation damage of polymers—III: synergism of heat and radiation on the chemorheology of ethylene-propylene rubber, *Radiat. Phys. Chem.* 17 (1981) 203.
- [52] M. Ito, Application of chemorheology to radiation damage of elastomer, *Int. J. Radiat. Appl. Instrum. C Radiat. Phys. Chem.* 31 (1988) 615.
- [53] M. Ito, Methodology Study of Qualification of Electric Wire and Cable Used in Nuclear Power Plant, Service Life Prediction of Polymeric Materials, Boston, MA, 2009.
- [54] M. Ito, Degradation of elastomer by heat and/or radiation, *Nucl. Instrum. Methods Phys. Res. B* 265 (2007) 227.
- [55] X. Colin, E. Richaud, J. Verdu, C. Monchy-Leroy, Kinetic modelling of radiochemical aging of ethylene-propylene copolymers, *Radiat. Phys. Chem.* 79 (2010) 365.
- [56] F. Djouani, Y. Zahra, B. Fayolle, M. Kuntz, J. Verdu, Degradation of epoxy coatings under gamma irradiation, *Radiat. Phys. Chem.* 82 (2013) 54.
- [57] N. Khelidj, X. Colin, L. Audouin, J. Verdu, C. Monchy-Leroy, V. Prunier, Oxidation of polyethylene under irradiation at low temperature and low dose rate. Part I. The case of "pure" radiochemical initiation, *Polym. Degrad. Stabil.* 91 (2006) 1593.
- [58] N. Khelidj, X. Colin, L. Audouin, J. Verdu, A simplified approach for the lifetime prediction of PE in nuclear environments, *Nucl. Instrum. Methods Phys. Res. B* 236 (2005) 88.
- [59] R.A. Assink, M. Celina, J.M. Skutnik, D.J. Harris, Use of a respirometer to measure oxidation rates of polymeric materials at ambient temperatures, *Polymer* 46 (2005) 11648.
- [60] M.C. Celina, A.R. Dayile, A. Quintana, A perspective on the inherent oxidation sensitivity of epoxy materials, *Polymer* 54 (2013) 3290.
- [61] K.T. Gillen, R. Assink, R. Bernstein, M. Celina, Condition monitoring methods applied to degradation of chlorosulfonated polyethylene cable jacketing materials, *Polym. Degrad. Stabil.* 91 (2006) 1273.
- [62] R. Bernstein, D.K. Derzon, K.T. Gillen, Nylon 6.6 accelerated aging studies: thermal-oxidative degradation and its interaction with hydrolysis, *Polym. Degrad. Stabil.* 88 (2005) 480.
- [63] S.G. Burnay, J. Dawson, Reverse temperature effect during ageing of XLPE cable insulation, in: L. Mallison (Ed.), *Ageing Studies and Life Extension of Materials*, Kluwer/Plenum Publishers, 2001.
- [64] H.J. Rudd, *Time Temperature Dose Rate Superposition Behavior in Irradiated Polymers*, Harwell Laboratory, Didcot, Oxon, UK, 1990. AERE-R13746.
- [65] Determination of long-term radiation ageing in polymers- Part 2: Procedures for predicting ageing at low dose rates, *Int. Electrotech. Comm.* (1996). IEC 1244-2.
- [66] Determination of long-term radiation ageing in polymers – Part 2: Procedures for predicting ageing at low dose rates, *Int. Electrotech. Comm.* (2014). IEC TS 61244-2.
- [67] K.T. Gillen, R. Bernstein, M. Celina, Non-Arrhenius behavior for oxidative degradation of chlorosulfonated polyethylene materials, *Polym. Degrad. Stabil.* 87 (2005) 335.
- [68] K.T. Gillen, R. Bernstein, D.K. Derzon, Evidence of non-Arrhenius behavior from laboratory aging and 24-year field aging of polychloroprene rubber materials, *Polym. Degrad. Stabil.* 87 (2005) 57.
- [69] P.Y. Le Gac, M. Celina, G. Roux, J. Verdu, P. Davies, B. Fayolle, Predictive ageing of elastomers: oxidation driven modulus changes for polychloroprene, *Polym. Degrad. Stabil.* 130 (2016) 348.
- [70] P. Gijsman, W. Dong, A. Quintana, M. Celina, Influence of temperature and stabilization on oxygen diffusion limited oxidation profiles of polyamide 6, *Polym. Degrad. Stabil.* 130 (2016) 83.
- [71] K.T. Gillen, Importance of synergism for combined radiation plus temperature environments, *Rubber Chem. Technol.* (2019) accepted, in press.